ATF3 Preserves Skeletal Muscle Stem Cell Quiescence by Preventing Precocious Activation

Suyang Zhang
The Chinese University of Hong Kong
Yile Huang
Department of Chemical Pathology, Li Ka Shing Institute of Health Sciences, The Chinese University of Hong Kong
Feng Yang
The Chinese University of Hong Kong
Liangqiang He
Chinese University of Hong Kong
Yuying Li
Chinese University of Hong Kong
Yi Ching Esther Wan
City University of Hong Kong
Yingzhe Ding
The Chinese University of Hong Kong
Kui ming Chan
City University of Hong Kong https://orcid.org/0000-0001-6430-3340
Ting Xie
The Hong Kong University of Science and Technology
Hao Sun
Chinese University of Hong Kong https://orcid.org/0000-0002-5547-9501
Huating Wang (huating.wang@cuhk.edu.hk)
The Chinese University of Hong Kong https://orcid.org/0000-0001-5474-2905

Article

Keywords: ATF3, muscle stem cell, quiescence, muscle regeneration, Histone 2B

Posted Date: September 6th, 2022

DOI: https://doi.org/10.21203/rs.3.rs-1982697/v1

ATF3 Preserves Skeletal Muscle Stem Cell Quiescence by Preventing Precocious Activation

Suyang Zhang[1,2], Yile Huang[3], Feng Yang[3], Liangqiang He[3], Yuying Li[3], Yi Ching Esther Wan[4,5], Yingzhe Ding[3], Kui Ming Chan[4,5], Ting Xie[6], Hao Sun[3,*] & Huating Wang[1,2,*]

1 Department of Orthopaedics and Traumatology, Li Ka Shing Institute of Health Sciences, Chinese University of Hong Kong, Hong Kong SAR, China.
2 Center for Neuromusculoskeletal Restorative Medicine, Hong Kong Science Park, New Territories, Hong Kong SAR, China
3 Department of Chemical Pathology, Li Ka Shing Institute of Health Sciences, Chinese University of Hong Kong, Hong Kong SAR, China.
4 Department of Biomedical Sciences, City University of Hong Kong, Hong Kong SAR, China.
5 Key Laboratory of Biochip Technology, Biotech and Health Centre, Shenzhen Research Institute of City University of Hong Kong, Shenzhen 518172, China.
6 Division of Life Science, The Hong Kong University of Science and Technology, Hong Kong SAR, China.
* These authors jointly supervised this work

Address correspondence to: Huating Wang, 507A Li Ka Shing Institute of Health Sciences, Prince of Wales Hospital, Chinese University of Hong Kong, Hong Kong SAR, China. Phone: (852)3763-6047; Fax: (852)-2632-0008; E-mail: huating.wang@cuhk.edu.hk

Hao Sun, R503, Li Ka Shing Institute of Health Sciences, Prince of Wales Hospital, Chinese University of Hong Kong, Hong Kong SAR, China. Phone: (852)3763-6048; E-mail: haosun@cuhk.edu.hk

Running title: ATF3 preserves muscle stem cell quiescence

Keywords: ATF3, muscle stem cell, quiescence, muscle regeneration, Histone 2B

Abstract

Skeletal muscle stem cells (also called satellite cells, SCs) are important for maintaining muscle tissue homeostasis and damage-induced regeneration. However, it remains poorly understood how the SC quiescence is preserved. Here we report that AP-1 family member ATF3 preserves the SC quiescence by preventing their premature activation. *Atf3* is rapidly and transiently induced in SCs upon activation. Short-term deletion of *Atf3* in SCs accelerates acute injury-induced regeneration, and however, its long-term deletion exhausts the SC pool and thus impairs muscle regeneration. The *Atf3* loss also provokes SC activation during voluntary exercise and enhances SC activation during resistance exercise. Mechanistically, ATF3 directly activates the transcription of *Histone 2B* genes, which reduction accelerates nucleosome displacement and gene transcription required for SC activation. Finally, the ATF3-dependent H2B expression also prevents genome instability and replicative senescence in SCs. Therefore, this study has revealed a novel mechanism for preserving the SC population by actively suppressing precocious activation, in which ATF3 is a key regulator.

Introduction

Muscle stem cells (also called satellite cells, SCs) are the adult stem cell population residing in the skeletal muscle, and play a key role in muscle tissue homeostasis and regeneration[1]. SCs normally lie quiescently beneath the muscle fiber between basal lamina and sarcolemma during homeostasis and are marked by expression of the paired box 7 (Pax7) transcription factor[2,3]. Upon muscle damage, SCs can rapidly exit the quiescence, enter the cell cycle to become activated and express myogenic determination factor 1 (MyoD); these activated SCs also known as myoblasts undergo proliferative expansion and differentiate into myotubes, which fuse into myofibers to repair the damaged muscle. Meanwhile, a subpopulation of SCs undergoes a self-renewal process and returns to the quiescent stage to replenish the SC pool. Each state of the myogenic lineage progression is orchestrated by complex regulatory networks consisting of intrinsic and extrinsic factors/mechanisms[4-9]. Disruption of the regulation may cause SCs to lose the ability to regenerate, contributing to muscle wasting conditions such as muscular dystrophy, cachexia, and sarcopenia. A key advance in our knowledge of SC biology in recent years is the revelation that both quiescence and the transition from quiescence into activation state are highly regulated. For example, upon minor muscle perturbation G_0 SCs can enter a G_{alert} or early activating stage which is characterized by enlarged size, enhanced mitochondrial activity and transcriptional activation. G_{alert} cells are thus primed for full activation once receiving the external stimuli[10]. Similarly, a report[11] defining the diversity in SCs also classifies quiescent SCs (QSCs) as genuine and primed populations based on CD34 expression level. Understanding the molecular underpinnings of these phases is undoubtedly essential to advance future therapies that can improve regenerative function of SCs, which however is hurdled by the technical difficulty in capturing their resident quiescent state. It is now widely accepted that the isolation processes involving mincing of the muscle, followed by enzymatic digestion and fluorescence-activated cell sorting (FACS) sorting will disturb or destroy the structure and microenvironment of niche, which will rapidly induce the adaptive response or early activation of SCs[12-14]. Pre-fixation of the tissue by Paraformaldehyde (PFA) before isolation is believed to preserve the quiescence of SCs to some extent. By comparing the pre-fixed and non-fixed SCs, a number

of reports[12-14] converge on the conclusion that SCs undergo massive changes in transcription and in fact enter an early activating stage during the isolation; one of the signature events occurring in the early response to the niche disruption is the rapid induction of Activation Protein-1 (AP-1) family members.

AP-1 transcription factors (TFs) regulate extensive cytological processes, such as proliferation, differentiation, apoptosis, angiogenesis and tumor invasion[15,16]. They are known to function as a dimeric complex that is composed of several monomers from JUN, FOS, ATF, BATF and MAF sub-families, all containing basic regions of bZIP (leucine-zipper) domains[17]. AP-1 family members are very sensitive to a variety of cellular stresses and quickly induced by even slight disturbance[18,19]. In response to the stress, these ATFs display critical roles in the signaling transduction and transcriptional regulation to further regulate cell fate decision, therefore constituting as one set of the most important and well characterized early response genes[20]. Among the AP-1 members, ATF3 belongs to the ATF sub-family and can repress and activate gene transcription, depending on the formation of homo or heterodimers with other ATF/CREB family members [21] and specific binding motifs on the promoter context[22,23]. Many studies have demonstrated that *Atf3* acts as a stress-inducible gene in rapid response to numerous stress conditions[24-37] and signaling pathways[38-43]. As a key immediate-early response gene with far-reaching impacts, it can act as an integration point for numerous cellular controls, working as a "hub" of the cellular adaptive–response network which is accountable for the disturbance of cellular homeostasis. Nevertheless, the functionality of ATF3 and other AP-1 family members in SCs remains unexplored.

In this study, we have delineated the function of ATF3 in SC quiescence preservation. It is rapidly and transiently induced upon exposure to external stimuli, such as tissue dissociation, physical exercise, and chemical-induced injury. Short-term deletion of *Atf3* from SCs causes SC activation which accelerates injury-induced regeneration, but long-term *Atf3* deletion leads to the depletion of SC pool and impairs further regeneration. Mechanistically, ATF3 binds to the promoter regions of *Histone2B* (*H2B*) genes to activate their expression; *Atf3*

deletion-induced H2B downregulation accelerates nucleosome displacement during transcription and thus up-regulates the genes involved in SC activation., The H2B loss also results in genome instability and enhanced replicative senescence in SCs. Thus, our findings have established ATF3 as a key factor for preserving the SC population by suppressing premature activation.

Results

ATF3 is rapidly and transiently induced during early SC activation

To explore the transcriptional regulatory events governing the SC quiescence-to-activation transition, we re-analyzed our previously published transcriptomic profiling datasets[44] acquired from SCs in the lineage progression. Briefly, muscles from *Pax7-nGFP* mice[45] were fixed in situ by PFA before subjecting to the standard 3hour (h) long cell dissociation and isolation process, and FACS sorting to obtain QSCs[13], or without prior fixation to obtain freshly isolated early activating SCs (FISC) (Fig. 1a); FISCs were cultured *in vitro* for 24h, 48h or 72h to obtain fully activated (ASC-24h), proliferating (ASC-48h) or differentiating (DSC-72h) cells. Consistent with the findings from other recent reports[46-48], AP-1 family genes including *Fos, Atf, Jun* and *Maf* sub-families were dramatically induced in FISCs compared to QSCs (Fig. 1b). Notably, *Atf3* was sharply induced (42.4 fold) in FISCs but was then rapidly decreased at ACS-24h (Fig. 1c-d); this was also confirmed by RT-qPCR (Fig. 1e), indicating that it is a rapid and transient responsive gene to early activation induced by the isolation. Furthermore, immunofluorescence (IF) staining demonstrated the concomitant induction of ATF3 protein in FISCs and a decrease in ASCs (Fig. 1f). Even on the freshly isolated single myofiber that is believed to preserve the quiescent niche to some extent and minimize SC activation[49,50], the associated SCs displayed high expression level of ATF3 protein immediately after 2h isolation which diminished at 24h in culture (Fig. 1g), reinforcing the notion that ATF3 is rapidly induced in early activated SCs. Several other AP-1 family members, *Atf4, Fos, FosB,* and *JunB*, shared a similar dynamic expression profile (Fig. 1b-d), which was also n confirmed by RT-qPCR (Fig. S1a) and immunofluorescent staining (Fig. S1b) results. Taken together, our findings show that ATF3 and several other AP-1 family members are rapidly and transiently induced during early SC activation, suggesting the potential roles of ATF3 and other family members in the regulation of SC quiescence or early activation.

Short-term *Atf3* deletion accelerates acute injury-induced muscle regeneration

To facilitate the dissection of ATF3 function in SCs, we crossed the $Atf3^{flox}$ allele[51], in

which two LoxP sites were inserted onto *Atf3* exon2, with *Pax7*$^{CreERT2/CreERT2}$-*R26R*$^{YFP/YFP}$ mouse[52] to generate control (Ctrl) (*Atf3*$^{+/+}$- *Pax7*$^{CreERT2/CreERT2}$-*R26R*$^{YFP/YFP}$) and inducible knockout mice of *Atf3* (*Atf3* iKO) (*Atf3* $^{flox/flox}$- *Pax7*$^{CreERT2/CreERT2}$-*R26R*$^{YFP/YFP}$) (Fig. 2a). After consecutive 5 days of intraperitoneal (IP) injection of Tamoxifen (TMX) (Fig. 2b), successful deletion of ATF3 in FISCs was confirmed by WB (Fig. 2c) or IF (Fig. S2a); its depletion was further confirmed by IF staining of SCs on single myofibers (Fig. S2b). Morphologically, the 2-month-old iKO showed no apparent difference from the Ctrl littermate mice; no changes in body size and weight were detected either (Fig. 2d).

Considering the rapid induction of ATF3 during early SC activation, we reasoned that its loss might impact on SC-mediated muscle regeneration. To test this notion, $BaCl_2$ was injected into the Tibialis Anterior (TA) muscles of Ctrl or iKO mice to induce acute muscle damage 5 days after TMX deletion (Fig. 2b). In this injury model[44,52,53], tissue degeneration with abundant immune cell infiltrates is normally observed at 1 day post injury (dpi); SCs are rapidly activated to expand as proliferating myoblasts which then fuse to form small new myofibers expressing embryonic myosin heavy chain (eMyHC) and characterized by centrally localized nuclei (CLN); these eMyHC+ fibers are readily seen at 5dpi. At 7dpi, the muscle is mainly composed of larger regenerated myofibers with down-regulated eMyHC expression; muscle damage and inflammatory cells are largely cleared at 14dpi while the regenerated myofibers continue to grow in size and mature to achieve full regeneration around 30dpi. By examining the above injured TA muscles at 3, 5, 7 and 30 dpi (Fig. 2b), the iKO muscles displayed a highly accelerated rate of regeneration. By H&E staining (Fig. 2e), at 5dpi, regenerating fibers with CLNs were already present in the iKO but not the Ctrl muscles. At 7dpi the damaged muscle was nearly repaired with homogenous fibers and no sign of immune cells in the iKO and the fiber size was also significantly larger compared to the Ctrl (the quantification on the right). These experimental observations were further supported by IF staining of eMyHC (Fig. 2f); eMyHC+ fibers were readily observed in the iKO even at 3dpi (89.63 in iKO vs 27.13 in Ctrl) but sharply decreased by 7dpi. In addition, the TA muscles collected from the iKO mice at 30 dpi had increased muscle weight compared to the Ctrl

(49.6 vs. 44.1mg) (Fig. S2c) and enlarged muscle fiber size (1089.2 vs. 828.7μm^2) (Fig. S2d), reflecting the enhanced repair.

Surprisingly, the enhanced regenerative ability of *Atf3* iKO SCs persisted after one more round of $BaCl_2$-induced acute injury given one month later (Fig. 2b). As shown in Fig. 2g-h, the accelerated regeneration remained equally strong based on the increased fiber size at 7dpi and the number of eMyHC+ fibers at 3dip after the 2nd injury. The 3rd round of injury was then given (Fig. 2b) and the expedited repair was still evident (Fig. 2i-j), as the number of eMyHC+ fibers at 3 dpi was still higher in the iKO vs. Ctrl muscles (89.9 vs. 45.7) (Fig. 2j) and a higher number of larger fibers was observed at 7dpi (Fig. 2i). However, despite slightly increased TA muscle weight in the iKO compared to the Ctrl 30d post-3rd injury (Fig. S2e), there was no significant difference in the average muscle fiber size (Fig. S2f), suggesting that the accelerated regeneration in the iKO muscle eventually disappeared after the 3rd injury. Consistently, the number of Pax7+ SCs was significantly reduced in the iKO compared to the control 30 d post-3rd injury (Fig. 2k).

The engraftment assay was then conducted to further validate the enhanced regenerative ability of the iKO SCs. As illustrated in Fig. 2l, twenty-one days after YFP+ SCs from the Ctrl or iKO mice were injected into the pre-injured TA muscles of receptor nude mice, the TA muscles were collected to evaluate donor cells' regenerative ability based on YFP expression. Indeed, we observed a higher number of YFP+ myofibers in the receptor mice transplanted with the iKO vs. Ctrl SCs (Fig. 2m). Altogether, our results demonstrate that *Atf3* deletion enhances acute injury-induced muscle regeneration.

Atf3 deletion provokes premature SC activation and pseudo-regeneration in homeostatic muscle

To dissect the underlying cause for the improved regenerative capacity upon ATF3 loss, we speculated that the iKO SCs underwent rapid activation upon $BaCl_2$ injury. Indeed, when plotting the dynamics of MyoD+ SCs along the course of the three rounds of

injury/regeneration. a much higher number of MyoD+ cells were detected at 3 dpi (Fig. 2n-o), but the cell number quickly declined at 5 dpi. Such phenomenon existed during the first two rounds of injury but disappeared in the third round (Fig. 2n-o). Compared to the Ctrl, the faster activation of iKO cells upon acute injury implies the quicker transition from quiescence to activation. Indeed, FISCs from the *Atf3*-iKO mice displayed a strikingly increased propensity for cell cycle entry based on EdU incorporation 24 h after culture (~23% increase) (Fig. 3a). In addition, Pax7+MyoD+ cells in the iKO exhibited 9% increase compared to the Ctrl 24h after culture (Fig. 3b). Furthermore, the FISCs from the iKO muscles were also slightly larger in size than the Ctrl ones (85.9 vs. 74.2) (Fig. 3c). Consistently, isolated single myofibers from the iKO muscles had significantly higher EdU incorporation (14% increase) than the Ctrl ones 36h after culture (Fig. 3d), reinforcing the faster cell cycle entry of the iKO SCs. The iKO SCs on freshly isolated single myofibers also produced 2.65-fold and 2.85-fold more Pax7+MyoD+ cells than those Ctrl SCs without culturing or with 3h (Fig. 3e-f). Altogether, these results indicate that the loss of ATF3 results in the release from quiescence and thus rapid SC activation without acute injury.

The enhanced regenerative ability of iKO SCs prompted us to further test if the ATF3 loss may lead to spontaneous activation and pseudo-regeneration in muscles without injury. Compared to the Ctrl, there was no increase of Pax7+ SCs in the iKO TA muscles at 5 days post-TMX injection but a significant increase of Pax7+ cells in the iKO TA muscles at 21 (14.5 vs. 9.5) and 28 days (11.4 vs. 8.9) (Fig. 3g), indicating the occurrence of spontaneous activation and expansion of iKO SCs in homeostatic muscles. Interestingly, by 56 days post-TMX injection, the number of Pax7+ cells in the iKO muscles finally declined compare to the Ctrl (Fig. 3g); this was accompanied by readily seen CLN+ fibers (Fig. 3h), indicating the fusion of the activated SC-derived myoblasts to existing fibers, which is known as pseudo-regeneration[54]. To confirm these findings, we performed five doses of EdU injection at 5 days post-TMX injection to show that there were more EdU+ cells on the muscle sections of the iKO than the Ctrl at 21 days post-EdU injection (Fig. 3i). Similarly, with a single dose of EdU administrated, EdU+ cells were only detected on the isolated iKO myofibers or TA muscles

12h later but not on the Ctrl ones (Fig. 3j). Altogether, these results suggest that *Atf3* deletion provokes the precocious activation of SCs in homeostatic muscles.

In addition, we observed there was 24% increase of MyoD+ MyoG+ differentiating cells in the isolated iKO muscle fibers compared to the Ctrl after 72h culture (Fig. 3k), suggesting that *Atf3* deletion may accelerate SC progeny differentiation. This was confirmed by staining for MyoD and MyoG on SCs cultured for 72h; 8% increase in the double positive cells was detected in the iKO vs. Ctrl (Fig. S3a). Interestingly, there was also a slight decrease of Pax7+MyoD- cells in the iKO muscle fibers compared to the Ctrl (10.13% vs 8.48%) (Fig. 3l). Along with the result from Fig. 2k, these results suggest that the loss of ATF3 might disrupt SC self-renewal.

Long-term *Atf3* deficiency depletes SC pool and impairs muscle regeneration

Next, to test if long-term *Atf3* deficiency causes SC exhaustion and impairs muscle regeneration, we induced muscle injury by $BaCl_2$ administration 30d or 120d after deleting *Atf3* from SCs and examined the injured TA muscles at 3d, 5d and 7dpi (Fig. 4a). Thirty days after the deletion, the muscle regeneration (based on the muscle fiber size and the eMyHC+ fiber number) showed no significant changes compared to the Ctrl mice (Fig. 4b-c). The number of Pax7+ SC was also comparable at 3 and 7 dpi and only slightly lower in the iKO at 5dpi (Fig. 4d). In contrast, 120d after the deletion, the muscle regeneration was obviously compromised in the iKO compared to the Ctrl mice. A significant increase of smaller fibers was observed at 7 dpi (Fig. 4e); the number of eMyHC+ fibers was much lower at 5dpi but higher at 7dpi (Fig. 4f); the number of Pax7+ SCs was also significantly reduced at both 3 and 7dpi (Fig. 4g). These results demonstrate that the long-term *Atf3* deficiency is detrimental to regeneration by shrinking the SC pool.

To further establish the importance of *Atf3* in SC establishment and maintenance, we successfully deleted *Atf3* in Pax7+ myogenic progenitors by crossing the $Atf3^{flox}$ allele with a non-inducible $Pax7^{Cre}$-$R26R^{YFP}$ transgenic mouse strain[55], in which the Cre recombinase is

expressed in Pax7+ progenitor cells in as early as E9.5 (Fig. S4a-c). Interestingly, the cKO muscles exhibited 84% increase of Pax7+ SCs compared to the Ctrl around one month after birth when SC pool was established[56], but 79% decrease in two-month-old adult mice (Fig. S4d), indicating that ATF3 is required for SC maintenance at adulthood but dispensable for SC establishment. Indeed, when the adult SCs were isolated and cultured, cKO cells displayed a much higher propensity for activation assessed by both Pax7+Myod+ staining (Fig. S4e, 23.8% increase in cKO vs. Ctrl) and EdU assay (Fig. S4f, 99.9% increase). Correspondingly, the regenerative capacity after acute injury was evidently compromised in cKO muscles (Fig. S4g-i). Therefore, the loss of ATF3 induces precocious SC activation and leads to the eventual reduction of the SC pool.

Atf3 deletion induces SC activation during voluntary and resistance exercises

Short term and non-strenuous voluntary exercise (VE) fails to cause SC activation but resistance exercise (RE) activates SCs[57-61]. To further prove the function of ATF3 in preventing SC activation, we sought to determine if the ATF3 depletion influences the VE-induced SC activation. Immediately after 5 doses of TMX injection, Ctrl and iKO mice were subject to an established voluntary wheel running regime; the mice were provided with access to free rotating running wheels; a stable VE routine was reached within 7 days of training and continued for another 21 days long (Fig. 5a). The daily running distance was recorded and no significant difference was detected between Ctrl (15.4 km) vs. iKO (14.5 km) mice (Fig. S5a-b).

Expectedly, the expressions of AP-1 family members were induced by the VE in Ctrl SCs (Fig. S5c). Also consistent with prior reports[61], the VE did not induce SC activation in the Ctrl mice as no MyoD+ cells were detected on the muscle sections before and after the VE (Fig. 5b); consistently, Pax7+MyoD+ staining of FISCs (Fig. 5c) or EdU staining of ASCs cultured for 24hr (Fig. 5d) did not reveal increased activation rate before and after the VE. In contrast, the iKO cells were readily activated by the VE (Fig. 5b-d). Consistently, in the iKO muscles, we also detected a significantly increased number of CLN fibers (136% increase) (Fig. 5e)

and evident hypertrophy (fiber size increased by 45.4%) after the VE (Fig. 5f). In the Ctrl muscles, the number of CLN was increased after the VE but not enough to cause hypertrophic growth (Fig. 5e-f). The above findings thus reinforce the notion that ATF3 loss induces rapid activation of SCs by the VE. As a result, there was reduced SC pool (29.2 % decrease of Pax7+ FISCs) at the end of the VE regime (Fig. 5g).

Since resistance exercise (RE) is known to cause SC activation and muscle hypertrophy[57-60], we next examined if the *Atf3* deficiency affects the RE-induced SC activation. To this end, Ctrl and iKO mice were subject to a treadmill running regime[62,63] in which the treadmill was set at a 5° incline and a speed of 20 cm/sec for 60min. After 5 doses of TMX injection, the mice were trained for a 5-day adaption period, then followed by a 10-day resistance training (+RE) or, as the control condition, without any training (-RE) (Fig. 5h). As expected, the expressions of AP-1 family members were rapidly induced by the RE in SCs (Fig. S5c). Furthermore, the RE caused evident SC activation in the Ctrl muscles, but the activation was much stronger in the iKO muscles (Fig. 5i-k). Consistently, CLN fibers were induced in both Ctrl and iKO muscles after the RE; and a higher increase of CLN fibers was seen in the iKO compared the Ctrl muscles (Fig. 5l). In addition, both Ctrl and iKO muscles showed hypertrophic growth after the RE but no difference was detected (Fig. 5m). At the end of the RE regime, the number of Pax7+ FISCs was significantly increased in the Ctrl but decreased in the iKO (Fig. 5n), indicating the rapid exhaustion of the iKO SC pool. Altogether, these findings indicate that the loss of ATF3 provokes the SC activation by VE and also enhances the SC activation by RE.

ATF3 regulates *H2B* gene expression and nucleosome patterning

Altogether the above results suggest an essential role of ATF3 induction in preventing precocious SC activation, to illuminate the underlying molecular mechanism, we profiled the ATF3 transcriptional output by performing RNA-Seq in FISCs collected from the Ctrl and iKO muscles (Fig. 6a). A total of 1866 transcripts (red dots) (79.9%) were up-regulated in the iKO compared to the Ctrl, while 469 (blue dots) (20.1%) were down-regulated (Fig. 6b, Fig.

S6a and Suppl. Table S1), suggesting that the ATF3 loss induced global transcriptional activation. The GO analysis revealed that the up-regulated genes were enriched for "mitochondrion" "extracellular matrix" etc. (Fig. 6c and Suppl. Table S1). Of note, elevated mitochondrial activity and extracellular matrix expression have previously been described in the G_{Alert} cells[10], suggesting that ATF3 functions to repress the expression of these activating genes, thus preventing premature SC activation. The down-regulated genes were interestingly enriched for "nucleosome" and "nucleosome assembly" etc. (Fig. 6d and Suppl. Table S1). Interestingly, the genes encoding Histone proteins were highly represented among the down-regulated genes (Fig. 6e), which was also confirmed by qRT-PCR (19-46% decrease) (Suppl. Fig. 6b). Histone encoding genes are typically organized into multigene clusters and H2B protein is encoded by 2 gene clusters with 15 on Chr13 forming a *Hist1h2b* cluster and 2 on Chr3 forming a *Hist2h2b* cluster (Fig. S6c). Remarkably, 13 out of the 17 *H2b* genes were down-regulated in the iKO SCs (Fig. 6e). Additionally, we also performed RNA-Seq on FISCs isolated from the Ctrl and *Atf3*-cKO mice and similar results were obtained (Fig. S6d-g and Suppl. Table S3). These results demonstrate that the ATF3 loss decreases *H2b* gene expression.

Next, we performed ChIP-Seq on the C2C12 myoblasts with exogenous ATF3 over-expression as a surrogate system to define direct binding targets of ATF3 (Fig. 6a and Fig. S6h). A total of 2871 binding peaks were identified in 869 genes with 60%, 28% and 9% located in intergenic regions, introns and promoters, respectively (Fig. 6f and Suppl. Table S2). These peaks were enriched for the known ATF3 binding motif, TGACTCA (Fig. 6g), attesting to the good data quality. GO analysis of these ATF3 bound genes indicated remarkable enrichment for the terms related to nucleosome (Fig. 6h and Suppl. Table S2). By integrating the RNA-Seq and ChIP-Seq results, 72 down-regulated genes contained ATF3 binding sites and again they were enriched for nucleosome related GO terms and many were histone genes (Fig. 6i and Suppl. Table S2). Notably, 8 of the 13 down-regulated *H2b* genes had ATF3 binding sites in their promoters (Fig. 6i-j, Fig. S6i and Suppl. Table S2). Meanwhile, 112 up-regulated genes possessed ATF3 binding and were enriched for

mitochondrion related GO terms (Fig. S6j and Suppl. Table S2). The Western blot (Fig. 6k) and IF staining (Fig. 6l) results confirmed a substantial reduction or near loss of H2B protein in the iKO FISCs while other histone proteins such as H3, H4 and H2A remained unaltered. These results demonstrate that *H2b* genes are bona fide transcriptional targets of ATF3.

Global diminution of histones leads to decreased amount of nucleosomes, augmented nucleosome spacing, and alters nucleosome occupancy thus affects transcription [64-66], to determine if the H2B loss in the iKO SCs alters of nucleosome positioning and occupancy, CUT&RUN assay[67,68] was performed to map the genomic localization of H2B in Ctrl and iKO cells (Fig. 6a). A total of 253,712 bins were defined genome-wide (Suppl. Table S4). Unexpectedly, the average H2B CUT&RUN signals were largely unaltered in the iKO vs. Ctrl with only 6598 bins (2.6%) showing changes (Fig. 6m-n). Nevertheless, 6369 out of the altered bins indeed showed decreased H2B enrichment in various genomic regions, including promoter (13%), gene body (30%) and intergenic regions (57%) (Fig. 6m). Since the nucleosome is partly dissembled through the removal of one H2A-H2B dimer to facilitate Pol II transcription[68] (Fig. 6o), we hypothesized that the local loss of H2B could facilitate nucleosome destabilization to promote the transcription of associated genes. Indeed, by intersecting with RNA-Seq data, 252 up-regulated genes showed decreased H2B signals on their promoters or gene bodies (Fig. 6p-q and Supp. Table S4). These genes were enriched for GO terms related to “extracellular matrix organization”, such as *Eln*, (Fig. 6r-s) which was consistent with the activation state of the iKO SCs. Taken together, these findings demonstrate that the decreased H2B level could mediate the precocious SC activation following the ATF3 loss.

H2B loss increases DNA damage and senescence in *Atf3* iKO SCs

To further elucidate the consequence of H2B loss in SCs, we examined genome instability and cellular senescence considering histone proteins are important for chromatin integrity and genome stability[64,66]. FISCs from iKO or Ctrl muscles were treated with various dosages (0, 1000 or 2000J) of UV light and comet assay was performed. Indeed, a substantial increase in

the comet tail length was observed under all three dosages in the iKO as compared to the Ctrl (Fig. 7a), suggesting that H2B decrease causes genomic instability. This was further confirmed by a much higher percentage of γH2AX+ cells in the cultured iKO cells compared to the Ctrl (Fig. 7b-c). To examine if the genomic instability leads to cellular senescence, cells were cultured in growth medium for 9 days and β-Gal staining was performed; a 19% increase of β-Gal+ cells was detected in the iKO compared to the Ctrl (Fig. 7d). Consistently, a significant up-regulation of *p16*, *p21*, and *p53* mRNAs (Fig. 7e) and a higher level of p21 and p53 proteins were also detected in the iKO (Fig. 7f). Altogether, the above findings demonstrate that H2B loss leads to increased genome instability and cellular senescence in the *Atf3* iKO cells. Expectedly, H2B over-expression in the iKO cells reduced the DNA damage accumulation and inhibited cellular senescence as assessed by decreased p21 protein (Fig. 7g) as well as *p16*, *p21* and *p53* mRNAs (Fig. 7h); Consistently, accelerated cell proliferation in the iKO was also curbed (Fig. 7I, 8.4% reduction of EdU+ cell). These results indicate that the decreased H2B expression causes SCs to undergo replicative senescence.

Screening of other functional AP-1 family members in SCs and regeneration.

After the above holistic characterization of the function and mechanism of ATF3 in SCs, we sought to expand the study by asking if other AP-1 family TFs such as ATF4, FOS, FOSB, and JUNB, also play functional roles in SCs considering their similar rapid and transient induction dynamics during SC early activation (Fig. 1b-d, S1b). To test the idea, we conducted a functional screening using our recently developed $Pax7^{Cas9}$/AAV-sgRNA mediated in vivo genome editing platform[69], which is based on a Cre-dependent Cas9 knock-in mice and AAV-mediated sgRNAs delivery. Briefly, one pair of sgRNAs targeting each TF were selected and packaged into AAV9 virus particles; 4×10^{11} viral genomes (vg)/mouse of AAV9-sgRNA was intramuscularly (IM) injected into the TA muscle of $Pax7^{Cas9}$ mouse at postnatal (P) age of 10 days (P10). For the control (Ctrl) group, the same dose of AAV9 virus containing pAAV9-sgRNA vector backbone without any sgRNA insertion was injected. The mice were then sacrificed for SC isolation and analysis after eight weeks (Fig S7a). Successful DNA editing efficiency was confirmed for all four TFs (Fig. S7b-e); consistently,

knock down (KD) of each protein to various degrees (52.4%-83.6%) was detected by WB (Fig. S7b-e) or IF (Fig. S7f) despite unaltered mRNA levels (Fig. S7g).

To examine the effect of the above AP-1 TF KD on SC activation, FISCs from each mutant were cultured for in vitro EdU assay (Fig. S7a). Similar to *Atf3* KO, the *Fos*-KD cells showed accelerated SC activation while the *JunB*-KD displayed blunted activation; the *Atf4* or *FosB*-KD, on the other hand, did not have any impact (Fig. S7h). When measuring Pax7+ cells on ~2 month-old uninjured muscles, interestingly, reduced numbers were observed upon the *Atf4*, *Fos* or *JunB*-KD (Fig. S7i), suggesting a loss of SC pool. Since the *Atf4* or *JunB*-KD did not lead to precocious SC activation, the SC number loss may be caused by other reasons considering the deletion occurred very early in the postnatal stage[69]. The *FosB*-KD did not have any impact on the Pax7+ SC pool.

To further investigate the impact on muscle regenerative ability, $BaCl_2$ was injected 7 weeks after AAV injection (Fig. S7a) and the regeneration was assessed by H&E (Fig. S7j), eMyHC (Fig. S7k), Pax7 (Fig. S7l) and MyoD (Fig. S7m) staining at 5dpi. An impaired regeneration was revealed in the *Atf4* and *Fos*-KD presumably because of the exhaustion of SCs after its long-term deletion; The regeneration in the *JunB*-KD was also compromised probably due to a reduced SC pool; consistently, no impact on the regeneration was observed in the *FosB*-KD. Altogether, our results that these AP-1 family members may play diverse functions in SC activation and muscle regeneration.

Discussion

In this study, we have elucidated the functional role of ATF3 in preventing premature activation and preserving the quiescence of SCs in the mouse skeletal muscle. ATF3 and other AP-1 family members exhibit rapid and transient induction in SCs upon isolation induced early activation. Interestingly, the inducible *Atf3* deletion in SCs causes their precocious activation and thus accelerates acute-injury induced regeneration, but the long-term *Atf3* depletion causes the exhaustion of the SC pool in the homeostatic muscle and thus impairs its regeneration. The loss of ATF3 also provokes SC rapid activation during voluntary exercise and further enhances SC activation during resistance exercise. Mechanistically, ATF3 binds and directly regulates the transcription of Histone2B (H2B); the *Atf3* ablation leads to H2B downregulation, which accelerates nucleosome displacement during transcription and thus upregulates the genes involved in SC activation. The H2B loss also results in genome instability and enhances replicative senescence in SCs. Lastly, a functional screening uncovers that several other AP-1 family TFs may also play diversified functions in SC activation and acute damage induced muscle regeneration. Therefore, this study has revealed a novel role of ATF3 in SCs for preventing premature activation, thereby maintaining the SC pool and regenerative ability (Fig. 7j).

The competence of SCs to drive robust tissue regeneration is based on their ability to exit from their steady-state quiescent stage and pass to an activated state following stimuli encountered notably in traumatic or pathological conditions. Recent technical advances have permitted the exploration of both quiescence and activation and revealed a high level of complexity in the molecular regulation of these stages[12-14]. It is widely accepted that during mechanical enzymatic tissue dissociation, SCs undergo massive changes in transcription and histone modifications in fact enter an early activating stage; one of the signature events occurring in the early response to the disruption of their niche is the prominent induction of AP-1 members[12-14]. Our expression profiling recapitulates the early responsive nature of ATF3/AP-1: its rapid (within hours) and transient induction in SCs upon exposure to external stimuli including chemical/mechanical dissociation coupled with FACS-based purification, isolation of intact single muscle fibers, exercise-induced micro-trauma, and chemically

induced muscle damage *in vivo*. The rapid induction of ATF3 upon stress induced by disrupting SC niche maintenance seemingly indicates a promoting role of ATF3 in the transition of SC quiescence to activation, it was thus surprising to observe a complete opposite phenotype upon deletion of *Atf3*. ATF3 loss clearly renders SCs to break quiescence and enter an early stage of activation even in the undisrupted homeostatic muscle. These cells can rapidly proceed to full activation once receiving stimuli from the growth medium in culture or acute injury in vivo. In the acute damage induced muscle regeneration, this ability endows iKO SCs with enhanced regenerative potential; even with three rounds of injuries, iKO SCs still managed to achieve full regeneration of the damaged muscle. The precocious activation of iKO SCs was also confirmed in exercise settings. SCs have been implicated in exercise induced muscle growth but their exact contribution and mechanisms remain under explored due to the many variables in exercise settings. Despite the voluntary exercise regimen did not cause SC activation in Ctrl mice, iKO SCs displayed evident activation and contribution to muscle hypertrophy growth in this type of exercise. In the more strenuous resistance exercise, iKO SCs expectedly showed enhanced activating ability than Ctrl cells. It is not surprising that these iKO cells could easily undergo pseudo-regeneration in which they enter full activation, differentiation and fuse with fibers to deposit their nuclei centrally even without acute injury, therefore, depletion of SC pool occurred with long term deficiency of ATF3, rendering the regeneration impaired. Altogether, our findings demonstrate the early activating status of iKO SCs thus exalted activating ability under various stimuli in multiple settings, therefore, the rapid induction of ATF3 in SCs by various stress signals appears to function to actively suppress the cells from proceeding to activation. This therefore sets ATF3 distinct from previously characterized quiescence-maintaining factors that are usually highly expressed in QSCs to actively preserve the quiescent state; these factors include Notch[70-73], FoxO[11] or Rac[74] signaling, etc. Its function is also in contrast to those rapidly induced to facilitate the transition from quiescence to early activation such as Fos[48], mTORC1[10], or PI3K signaling[47]. In the homeostatic muscle, we believe ATF3 induction by minor stress such as stretching, exercise-induced-micro-trauma, etc. thus serves to actively suppress activating program to preserve the deep quiescence of SCs. If exposed to more severe myofiber

destruction such as $BaCl_2$ induced acute injury, the cells will need to down-regulate ATF3 and proceed with activation; a small subset of cells probably preserves the expression of ATF3 and stemness and contribute to self-renewal in the later phase of regeneration. Consistently, we observed defect in self-renewal of iKO SCs after each round of three injuries. Of note, coincident with our theory, a recent report[75] shows that ATF3 plays an important role in maintaining hematopoietic stem cells (HSCs) self-renewal and preventing stress-induced exhaustion of HSCs. Similarly, ATF3 deficiency leads to enhanced proliferation of HSCs under short-term stress but causes long-term exhaustion after long-term stress exposure. Therefore, it is possible that ATF3 plays previously unappreciated roles in stem cell homeostasis and regeneration in general.

To fathom the underlying mechanism of how ATF3 executes the above described functions in SCs, integrating RNA-Seq and ChIP-Seq, our findings uncovered interesting binding and regulation of ATF3 on Histone 2 transcription. Compared to the wealth of transcriptional regulatory mechanism of histone gene expression in budding yeast, much needs to be learned in mammals[65,66,76,77]. Here our findings revealed the direct transcriptional regulation of both clusters encoding *H2b* genes by ATF3. The binding of ATF3 on the divergent promoters of *H2b* genes on both chromosome 13 and 3 enables simultaneous regulation of a histone gene pair. Proper histone gene expression and histone protein synthesis are key to nucleosome assembly and composition which in turn governs chromatin structure and gene transcription. Rapid induction of ATF3 under stress may thus function to ensure H2B protein production and proper nucleosome organization for controlling the expression of genes to prevent cell activation. Loss of ATF3 expectedly caused an obvious loss of H2B protein in SCs, which interestingly did not result in genome-wide decrease of H2B enrichment by CUT&RUN, suggesting genome-wide nucleosome occupancy may not be largely impacted. It is likely the reduced amount of H2B may lead to formation of non-canonical nucleosomes[78], for example, so called half-nucleosomes consisting of one copy of each of the four core histones or hexasomes with two copies of H3/H4 and one copy of H2A/H2B. These possibilities can be investigated in detail in the future by additional approaches such as MNase digestion etc. The

function of these subnucleosomes in transcription is still unclear, it is possible that they prevalently exist in the iKO cells and alter the overall nucleosome structure and chromatin properties, therefore explaining the overall transcriptional activation occurring in the cell. In addition, the existence of these subnucleosomes may also affect genomic stability and increase the propensity for DNA damage thus cellular senescence, which was indeed observed in the iKO cells (Fig. 7). Aging-coupled histone loss also results in elevated levels of DNA strand breaks and genomic instability in budding yeast[76,77], it will thus be interesting to examine whether ATF3 loss will accelerate SC aging which is known to contribute to muscle tissue aging[79-81].

In addition to ATF3, several other AP-1 family members showed rapid induction in FISCs, suggesting their potential functionality in the transition from quiescence to early activation. Indeed, the in vivo functional screening revealed rather diversified roles of ATF4, FOS, FOSB and JUNB in SC activation and muscle regeneration. While ATF4 and FOS appear to play similar functions as ATF3 in preserving SC quiescence and preventing precocious activation, JUNB may have an opposite action. FOSB loss, on the other, did not have detectable effect on SCs in the screening. Indeed, Wang G *et al*[47] demonstrates that c-Jun is a key transcriptional target of the PI3K/mTORC1 signaling axis essential for SC quiescence exit upon muscle injury. Taglietti V *et al*[46]also shows that JUNB is an activator of fetal myogenesis. Nonetheless, it is interesting to point out that a recent study[48] demonstrates that rapid and transient induction of FOS is required to direct SC early activation events needed for efficient regeneration. FOS is found to be heterogeneously induced in a subset of SCs which exhibit a greater propensity for entering the early stages of activation. Loss of FOS in SCs thus impairs their capacity to enter the cell cycle. We suspect the discrepancy from our study could arise from the different systems used to delete FOS. In our system Cas9 is expressed not only in SCs but also muscle fibers of the $Pax7^{Cas9}$ mice, thus impossible to achieve inducible SC specific deletion[69]. In addition, the editing efficiency per SC and the editing events largely varied[69], leading to mosaic mutagenesis. It is also possible that ATF3 is mainly induced in the subset of SCs with high propensity for deep quiescence and self-renewal while FOS is

expressed in a subset of SCs with a greater propensity for entering the early stage of activation. Loss of ATF3 in the subset of SCs provokes them to become pro-activating and regenerative. This reinforces the increasingly recognized molecular and functional heterogeneity within the SC population which equips the cells with adaptive potentials in response to different demands[10].

Methods

Animal studies

All animal handling procedures, protocols and experiments ethics approval was granted by the CUHK AEEC (Animal Experimentation Ethics Committee) under the Ref No. 16-166-MIS and 21-254-MIS. The mice were maintained in animal room with 12 h light/12 h dark cycles, temperature (22–24 °C), and humidity (40–60%) at animal facility in CUHK. For all animal-based experiments, at least three pairs of littermates or age-matched mice were used.

The Tg: *Pax7-nGFP* mouse strains[45], $Pax7^{CreER}$ ($Pax7^{tm1(cre/ERT2)Gaka}$)[82]; $ROSA^{EYFP}$ reporter mice and $Pax7^{Cre}$ ($Pax7^{tm1(cre)Mrc}$)[55]; $ROSA^{EYFP}$ reporter mice were kindly provided by Dr. Zhenguo WU (Hong Kong University of Science and Technology). The $Atf3^{fl/fl}$ mouse strain was kindly provided by Prof. Tsonwin HAI (Ohio State University, USA)[51]. The C57BL wildtype mice were purchased from LASEC (Laboratory Animal Services Centre) of CUHK. The *Atf3* inducible conditional KO mice (*Atf3* iKO) with EYFP reporter (Ctrl: $Pax7^{CreER/+}$; $ROSA^{EYFP/+}$; *Atf3*+/+, iKO: $Pax7^{CreER/+}$; $ROSA^{EYFP/+}$; $Atf3^{fl/fl}$) were generated by crossing $Pax7^{CreER}$; $ROSA^{EYFP}$ with $Atf3^{fl/fl}$ mice. The *Atf3* conditional KO mice (*Atf3* cKO) with EYFP reporter (Ctrl: $Pax7^{Cre/+}$; $ROSA^{EYFP/+}$; *Atf3*+/+, cKO: $Pax7^{Cre/+}$; $ROSA^{EYFP/+}$; $Atf3^{fl/fl}$) were generated by crossing $Pax7^{Cre}$; $ROSA^{EYFP}$ with $Atf3^{fl/fl}$ mice. To induce Cre-mediated *Atf3* deletion, Tamoxifen (TMX) (T5648, Sigma) was injected intraperitoneally at 2 mg per 20 g body weight for consecutive 5 days. The $Pax7^{Cre}$ dependent $Rosa26^{Cas9\text{-}EGFP}$ knock-in mice were generated as described[69]. Primers used for genotyping are shown in Suppl. Table 5.

To induce acute muscle injury, 50 µl of 1.2% $BaCl_2$ (dissolved in sterile demineralized water) was injected into TA muscle of age-appropriate mice. Muscles were harvested at designated time points for subsequent histological or biochemical studies. For in vivo EdU incorporation assay, 10mg EdU diluted in 100ul PBS was injected intraperitoneally, TA muscles and myofibers were harvested 12 hours later, or 0.6mg EdU diluted in 100ul PBS were IP injected for consecutive 5 days; TA muscles and myofibers were harvested 21 days later, followed by 4% PFA fixation. EdU-labeled cells were visualized using click chemistry with an Alexa Fluor® 594 conjugated azide. Images were captured with a fluorescence microscope (Leica).

For the voluntary wheel running exercise, mice were housed individually for 4 weeks in

polycarbonate cages with 12-cm-diameter wheels equipped with optical rotation sensors (Yuyan Instrument, ARW) After 5 doses of TMX injection, the mice were firstly trained by the above settings for 7 days and followed by consecutive 21 days of exercise. For resistance exercise, mice were adapted to a treadmill (Panlab, Harvard Apparatus, 76-0895) with a 5° incline at a speed of 20 cm/sec for 60min. After 5 doses of TMX injection, the mice were firstly trained by the above settings for 5 days and followed by consecutive 10 days of exercise. For non-exercised control, mice were housed individually in standard polyethylene cages without access to any exercise wheel or treadmill.

CRISPR/Cas9 mediated in vivo genome editing

The in vivo genome editing via CRISPR/Cas9 was performed according to previously described instructions[69]. Briefly, Cre-dependent $Pax7^{Cas9}$ mouse was generated through crossing $Pax7^{Cre}$ mouse[55] with homozygous $Rosa^{Cas9\text{-}eGFP}$ mouse[83], resulting in the labeling of all Pax7 derived cells (muscle lineage) with eGFP. In vitro validated sgRNA pairs targeting each AP-1 family TF were generated from a U6-driven AAV9 backbone using muscle-tropic AAV9 as the delivery vector. The $Pax7^{Cas9}$ mice were injected intramuscularly with a single dose (5×10^{11} vg per mouse) of AAV9-sgRNA at postnatal day 10 (P10) and were analyzed 8 weeks later.

Satellite cell isolation and culture

Satellite cells were sorted based on established methods[84]. Briefly, entire hindlimb muscles from mice were digested with collagenase II (LS004177, Worthington, 1000 units per 1ml) for 90 min at 37°C, the digested muscles were then washed in washing medium (Ham's F-10 medium (N6635, Sigma) containing 10% horse serum, heat-inactivated (HIHS, 26050088, Gibco, 1% P/S) before SCs were liberated by treating with Collagenase II (100 units per 1ml) and Dispase (17105-041, Gibco, 1.1 unit per 1ml) for 30 min. The suspensions were passed through a 20 G needle to release myofiber-associated SCs. Mononuclear cells were filtered with a 40-μm cell strainer and sorted by BD FACSAria IV (fluorescence-activated cell sorting) with the selection of the positive GFP fluorescence signal. Coverslips and cultural

wells were coated with poly-D-lysine solution (p0899, Sigma) at 37 °C for overnight and then coated with extracellular matrix (ECM) (E-1270, Sigma) at 4 °C for at least 6 h. FACS-isolated SCs were seeded in coated wells and cultured in Ham's F10 medium with 10% HIHS, 5 ng ml−1 β-FGF (PHG0026, Thermo Fisher Scientific) and 1% P/S.

Single myofiber isolation and culture

As described before[85,86], single myofibers were isolated from the EDL (extensor digitorum longus) muscles of adult mice. The EDL was dissected and digested in the digestion solution (800U Collagenase type II in 1ml DMEM medium) at 37 °C for 75 minutes with a shake of 70 rpm. After digestion, the single myofibers were released by gentle trituration with Ham's F-10 medium containing 10% HIHS and 1% P/S and cultured in this medium for designated time points.

Cell line culture

C2C12 mouse myoblast cell line was obtained from ATCC (American Type Culture Collection) and cultured in DMEM medium (Gibco, 12800-017) with 10% FBS (fetal bovine serum, Gibco, 10270-106) and 1% P/S (Penicillin-Streptomycin, 10,000U/ml, Gibco,15140-122) at 37℃ in cell incubator with 5% CO_2. The cells were induced to differentiate when they reached an 80-90% confluence, by altering the GM to DM (differentiation medium) which consisted of DMEM medium, 2% HS (Horse Serum, Gibco, 16050114) and 1% P/S under the same culture environment. Lentiviruses expressing sgRNSs of AP-1 family members were packaged in 293T cells as previously described[69].

Cell proliferation assay

EdU incorporation assay was performed following the instruction of Click-iT® Plus EdU Alexa Fluor® 594 Imaging Kit (C10639, Thermo Fisher Scientific). Growing cells on coverslips were incubated with 10 μM EdU for a designated time before the fixation with 4% PFA for 20 min. EdU-labeled cells were visualized using "click" chemistry with an Alexa Fluor® 594-conjugated azide and cell nuclei were stained by DAPI (Life Technologies,

P36931). Images were captured with a fluorescence microscope (Leica).

SA-β-galactosidase staining

Cellular senescence was evaluated by β-galactosidase activity using β-galactosidase Senescence Kit (Cell signaling, #9860) after being cultured for designated times. Briefly, satellite cells were fixed for 10-15 minutes followed by washing in PBS. The cells were then incubated with β-galactosidase staining solution at 37℃ at least overnight in a dry incubator without CO_2. The cells were then observed under a microscope for the development of blue color which represents the existence of β-galactosidase, a significant feature of senescent cells.

Comet assay

The alkaline comet assay was conducted to measure the DNA damage level in satellite cells. Sorted satellite cells were treated with UV radiation at different dosages and the comet assay was operated immediately after irradiation through a Comet Assay Kit (Abcam, ab238544) according to the manufacturer's instructions. The amount of DNA damage was indicated by the tail moment which is a measure of DNA fragments with a Leica fluorescence microscope.

Plasmids

To construct ATF3 expression plasmid, a 545 bp DNA fragment of *Atf3* CDS (coding DNA sequence) region was amplified and cloned into a pcDNA3.1+ vector between KpnI and XbnI. To construct H2B expression plasmid, a 493 bp DNA fragment of mouse *hist2h2bb* gene full-length was amplified and cloned into a pcDNA3.1+ vector between HindlllI and KpnI. To generate *Atf4*, *Fos*, *FosB* and *JunB* in vivo knockdown mice, two sgRNAs for each target gene were designed by CRISPOR[87] and cloned into PX458 vector at the BbsI site[69].

RNA extraction and qRT-PCR

Total RNAs from cells or tissues were extracted using TRIzol reagent (Invitrogen,

15596018) according to the manufacturer's instructions. cDNAs were synthesized under the manufacturer's instructions of HiScript® II Reverse Transcriptase Kit with gDNA wiper (Vazyme, R223-01). Real-time PCR was performed to quantify the expression level of mRNAs by Luna® Universal qPCR Master Mix (NEB, M3003E) and LightCycler ®480 Real-Time PCR System (Roche). GAPDH (glyceraldehydes 3-phosphate dehydrogenase) or 18s RNA were used as internal controls for normalization. The primers used were listed in Suppl. Table 1. The relative fold changes compared to control groups were calculated by the classical ΔΔCt method.

Immunoblotting, immunofluorescence, and immunohistochemistry

For Western blot, cells or tissues were harvested, washed with PBS, and lysed in RIPA buffer supplemented with protease inhibitor cocktail, PIC (88266, Thermo Fisher Scientific) for 30 min on ice. The protein concentration was determined using a Bradford protein assay kit (Bio-Rad). Whole-cell lysates were subjected to SDS–PAGE, and protein expression was visualized using an enhanced chemiluminescence detection system (GE Healthcare, Little Chalfont, UK) as described before[88]. The following dilutions were used for each antibody: ATF3 (Santa Cruz Biotechnology; 1:5,000), H2A (Abcam; 1: 2,500), H2B (Abcam; 1: 2,500), H3 (Santa Cruz Biotechnology; 1:4,000), H4 (Abcam; 1:2,000), α-tubulin (Santa Cruz Biotechnology; 1:5,000) and GAPDH (Santa Cruz Biotechnology;1:5000).

For immunofluorescence staining, cultured cells or myofibers were fixed in 4% PFA for 15 min and permeabilized with 0.5% NP-40 for 10 min. Then cells were blocked in 3% BSA for 1 h followed by incubating with primary antibodies overnight at 4 °C and secondary antibodies for one hour at RT. Finally, the cells or myofibers were mounted with DAPI to stain the cell nucleus and images were captured by a Leica fluorescence microscope. Primary antibodies and dilutions were used as following PAX7 (Developmental Studies Hybridoma Bank; 1:50), MyoD (Dako; 1: 1,000), MyoG (Santa Cruz Biotechnology; 1:200), ATF3 (Santa Cruz Biotechnology; 1:2,000), H2A (Abcam; 1:1,000), H2B (Abcam; 1:1,000), γ-H2AX (Biolegend; 1:200), ATF4 (Santa Cruz Biotechnology; 1:200), FOS (Santa Cruz Biotechnology; 1:200), FOSB (Santa Cruz Biotechnology; 1:200) and JUNB (Santa Cruz

Biotechnology; 1:200).

For immunohistochemistry, in brief, slides were fixed with 4% PFA for 15 min at room temperature and permeabilized in ice-cold menthol for 6 min at −20 °C. Heat-mediated antigen retrieval with a 0.01 M citric acid (pH 6.0) was performed for 5 min in a microwave. After 4% BBBSA (4% IgG-free BSA in PBS; Jackson, 001-000-162) blocking, the sections were further blocked with unconjugated AffiniPure Fab Fragment (1:100 in PBS; Jackson, 115-007-003) for 30 min. The biotin-conjugated anti-mouse IgG (1:500 in 4% BBBSA, Jackson, 115-065-205) and Cy3-Streptavidin (1:1250 in 4% BBBSA, Jackson, 016-160-084) were used as secondary antibodies. Primary antibodies and dilutions were used as follows PAX7 (Developmental Studies Hybridoma Bank; 1:50), MyoD (Dako; 1:500), eMyHC (Developmental Studies Hybridoma Bank; 1:200) and Laminin (Sigma; 1:800). All fluorescent images were captured with a fluorescence microscope (Leica).

H&E (Hematoxylin-eosin) staining on TA muscle sections was performed according to a protocol described before[89]. Section slides were first stained in hematoxylin for 10 mins followed by rinsing thoroughly under running tap water for at least 3 mins. Then section slides were immersed in 0.2% acid alcohol for 1s and immediately rinsed under running tap water. Next, section slides were stained in eosin for 2 mins followed by rinsing and dehydrating in graded ethanol and Xylene. Finally, slides were mounted by DPX and observed under a normal microscope.

RNA-Seq and data analysis

For RNA-Seq, RNAs from satellite cells were extracted by Trizol reagent and delivered to Beijing Genome Institute (BGI), Hong Kong with dry ice. Data released by BGI from sequenced fragments were mapped to mouse genome mm9[90] using TopHat. The abundance levels of transcripts were defined by cufflinks[91] in the form of FPKM (reads per kilobase per million reads mapped). Differentially expressed genes (DEGs) between samples were identified by the change of expression levels using a threshold of log2FoldChange > 2. ClusterProfiler[92] was used for the Gene Ontology (GO) analysis with Entrez gene IDs converted from DAVID[93] tool as inputs. The adjusted P or *P* values were reported with the

GO terms.

ChIP-Seq and data analysis

Briefly, cells were cross-linked in 1% formaldehyde and processed according to previously described[94]. 10 μg of antibodies against ATF3 (Santa Cruz Biotechnology), or normal mouse IgG (Santa Cruz Biotechnology) was used for immunoprecipitation. Immunoprecipitated genomic DNA was resuspended in 20 μl of water. For DNA library construction, a NEBNext® Ultra™ II DNA Library Prep Kit for Illumina® (NEB, E7645S) was used according to the manufacturer's instructions. Bioanalyzer analysis and qPCR were used to measure the quality of DNA libraries including the DNA size and purity. Finally, DNA libraries were sequenced on the Illumina Genome Analyzer II platform.

The raw data were first pre-processed by initial quality assessment, adaptors trimming, and low-quality filtering and then mapped to the mouse reference genome (mm9) using bowtie2[95], and only the non-redundant reads were kept. The protein DNA-binding peaks (sites) were identified using MACS2[96] with input (IgG) sample as the background. During the peak calling, the *P*-value cutoff was set to 0.001 for ATF3 ChIP-Seq experiment.

CUT &RUN and date analysis

CUT&RUN assay was conducted using 250,000 satellite cells with the CUT&RUN assay kit (Cell Signaling Technology, 86652,). In brief, FISCs were harvested and washed by cell wash buffer, then bound to concanavalin A-coated magnetic beads. Digitonin Wash Buffer was used for permeabilization. After that, cells were incubated with 5 μg of H2A or H2B antibody (Abcam) overnight at 4 °C with shaking. Then, cell-bead slurry was washed with Digitonin Wash Buffer and incubated with Protein A-MNase for 1 h at 4 °C with shaking. After washing with Digitonin Wash Buffer, CaCl2 was added into the cell-bead slurry to initiate Protein A-MNase digestion, which was then incubated at 4°C for half an hour. Then 2x Stop Buffer was added to the reaction to stop the digestion. CUT&RUN fragments were released by incubation for 30 min at 37 °C followed by centrifugation. After centrifugation, the supernatant was recovered, and DNA purification was performed by using

Phenol/Chloroform (Thermo). For DNA library construction, a NEBNext® Ultra™ II DNA Library Prep Kit for Illumina® (NEB, E7645S) was used according to the manufacturer's instructions. Bioanalyzer analysis and qPCR were used to measure the quality of DNA libraries including the DNA size and purity. Finally, DNA libraries were sequenced on the Illumina Genome Analyzer II platform.

The raw reads were first pre-processed by quality assessment, adaptors trimming, and low-quality filtering, and then were aligned to the mouse reference genome (mm9) using Bowtie2[95], and only-redundant reads were kept. For the analysis of genome-wide differential H2B enrichment, we calculated the mean signal for H2B within each bin with 10 kb using the function "multiBigwigSummary bins" in deeptools[97]. Threshold of 1.5-fold change was used to classify changed or unchanged bins between *Atf3*-iKO samples and WT samples. As for analyzing the differential H2B enrichment on promoter and gene body, we compared the signals on promoter and gene body between *Atf3*-iKO and WT samples with the Mann-Whitney U test. And the P-value < 0.05 and fold change > 1.5 were considered as significantly different.

Statistical analysis

Data were analyzed using GraphPad Prism (version 8; GraphPad Software, San Diego, CA). Data were represented as the average of at least three biologically independent samples ± SD. The statistical significance was assessed by the Student's two-tailed paired and unpaired t-test by Excel software. Significance was described as n.s, not significant; * $P < 0.05$; ** $P < 0.01$ and *** $P < 0.001$.

Data availability

RNA-Seq, ATF3 ChIP-Seq and H2B CUT&RUN data generated in this study have been deposited in Gene Expression Omnibus (GEO) database under the accession codes GSE205170, GSE205314, GSE205324 and GSE205548.

Author Contributions

Suyang Zhang designed and performed most experiments; Yile Huang, Feng Yang and Yingzhe Ding. analyzed RNA-Seq, ATF3 ChIP-Seq and H2B CUT&RUN data; Liangqiang He, Yuying Li and Ching Esther Wan provided technical supports; Kui Ming Chan supervised CUT&RUN assay; Hao Sun supervised computational analyses; Suyang Zhang, Yile Huang, Feng Yang, Ting Xie and Huating Wang wrote the manuscript, with inputs from all authors.

Acknowledgments

This work was supported by Collaborative Research Fund (CRF) from the Research Grants Council (RGC) of the Hong Kong (HK) Special Administrative Region, China (project code: C6018-19GF); General Research Fund (GRF) from RGC to H.W. (project codes: 14106521, 14100620, 14115319, and 14106518 to H.W.; 14120420, 14116918, 14120619 and 14103522 to H.S.); Health and Medical Research Fund (HMRF) from Health Bureau of HK to H.W. (project code: 08190626); the research funds from Health@InnoHK program launched by Innovation Technology Commission, the Government of HK to H.W.; the National Natural Science Foundation of China (NSFC) to H.W. (project codes: 82172436 and 31871304); NSFC/RGC Joint Research Scheme (project code: N_CUHK 413/18 to H.S.). Theme-based Research Scheme (TRS) from RGC (project code: T13-602/21-N); Area of Excellence Scheme (AoE) from RGC (project code: AoE/M-402/20).

References

1. Brack AS, Rando TA. Tissue-specific stem cells: lessons from the skeletal muscle satellite cell. *Cell stem cell.* 2012;10(5):504-514.
2. Gopinath SD, Webb AE, Brunet A, Rando TA. FOXO3 promotes quiescence in adult muscle stem cells during the process of self-renewal. *Stem Cell Reports.* Apr 8 2014;2(4):414-426.
3. Yamaguchi M, Watanabe Y, Ohtani T, et al. Calcitonin Receptor Signaling Inhibits Muscle Stem Cells from Escaping the Quiescent State and the Niche. *Cell Rep.* Oct 13 2015;13(2):302-314.
4. Beauchamp JR, Heslop L, Yu DS, et al. Expression of CD34 and Myf5 defines the majority of quiescent adult skeletal muscle satellite cells. *The Journal of cell biology.* Dec 11 2000;151(6):1221-1234.
5. Charge SB, Rudnicki MA. Cellular and molecular regulation of muscle regeneration. *Physiol Rev.* Jan 2004;84(1):209-238.
6. Cornelison DD, Wold BJ. Single-cell analysis of regulatory gene expression in quiescent and activated mouse skeletal muscle satellite cells. *Dev Biol.* Nov 15 1997;191(2):270-283.
7. Montarras D, Morgan J, Collins C, et al. Direct isolation of satellite cells for skeletal muscle regeneration. *Science.* Sep 23 2005;309(5743):2064-2067.
8. Seale P, Sabourin LA, Girgis-Gabardo A, Mansouri A, Gruss P, Rudnicki MA. Pax7 is required for the specification of myogenic satellite cells. *Cell.* Sep 15 2000;102(6):777-786.
9. Sherwood RI, Christensen JL, Conboy IM, et al. Isolation of adult mouse myogenic progenitors: functional heterogeneity of cells within and engrafting skeletal muscle. *Cell.* Nov 12 2004;119(4):543-554.
10. Rodgers JT, King KY, Brett JO, et al. mTORC1 controls the adaptive transition of quiescent stem cells from G0 to G(Alert). *Nature.* Jun 19 2014;510(7505):393-396.
11. García-Prat L, Perdiguero E, Alonso-Martín S, et al. FoxO maintains a genuine muscle stem-cell quiescent state until geriatric age. *Nature cell biology.* Nov 2020;22(11):1307-1318.
12. van den Brink SC, Sage F, Vértesy Á, et al. Single-cell sequencing reveals dissociation-induced gene expression in tissue subpopulations. *Nature Methods.* 2017/10/01 2017;14(10):935-936.
13. Machado L, Esteves de Lima J, Fabre O, et al. In Situ Fixation Redefines Quiescence and Early Activation of Skeletal Muscle Stem Cells. *Cell Reports.* 2017/11/14/ 2017;21(7):1982-1993.
14. van Velthoven CT, de Morree A, Egner IM, Brett JO, Rando TA. Transcriptional profiling of quiescent muscle stem cells in vivo. *Cell reports.* 2017;21(7):1994-2004.
15. Shaulian E, Karin M. AP-1 as a regulator of cell life and death. *Nature cell biology.* May 2002;4(5):E131-136.
16. Eferl R, Wagner EF. AP-1: a double-edged sword in tumorigenesis. *Nature reviews. Cancer.* Nov 2003;3(11):859-868.
17. Glover JN, Harrison SC. Crystal structure of the heterodimeric bZIP transcription factor c-Fos-c-Jun bound to DNA. *Nature.* Jan 19 1995;373(6511):257-261.

18. Garces de Los Fayos Alonso I, Liang H-C, Turner SD, Lagger S, Merkel O, Kenner L. The Role of Activator Protein-1 (AP-1) Family Members in CD30-Positive Lymphomas. *Cancers (Basel).* 2018;10(4):93.

19. Senba E, Ueyama T. Stress-induced expression of immediate early genes in the brain and peripheral organs of the rat. *Neurosci Res.* Nov 1997;29(3):183-207.

20. Wisdom R. AP-1: one switch for many signals. *Exp Cell Res.* Nov 25 1999;253(1):180-185.

21. Hai T, Hartman MG. The molecular biology and nomenclature of the activating transcription factor/cAMP responsive element binding family of transcription factors: activating transcription factor proteins and homeostasis. *Gene.* 2001/07/25/ 2001;273(1):1-11.

22. Chen BP, Liang G, Whelan J, Hai T. ATF3 and ATF3 delta Zip. Transcriptional repression versus activation by alternatively spliced isoforms. *J Biol Chem.* Jun 3 1994;269(22):15819-15826.

23. Hai T, Curran T. Cross-family dimerization of transcription factors Fos/Jun and ATF/CREB alters DNA binding specificity. *Proc Natl Acad Sci U S A.* 1991;88(9):3720-3724.

24. Allen-Jennings AE, Hartman MG, Kociba GJ, Hai T. The roles of ATF3 in glucose homeostasis. A transgenic mouse model with liver dysfunction and defects in endocrine pancreas. *The Journal of biological chemistry.* Aug 3 2001;276(31):29507-29514.

25. Amundson SA, Bittner M, Chen Y, Trent J, Meltzer P, Fornace AJ, Jr. Fluorescent cDNA microarray hybridization reveals complexity and heterogeneity of cellular genotoxic stress responses. *Oncogene.* Jun 17 1999;18(24):3666-3672.

26. Cai Y, Zhang C, Nawa T, et al. Homocysteine-responsive ATF3 gene expression in human vascular endothelial cells: activation of c-Jun NH(2)-terminal kinase and promoter response element. *Blood.* Sep 15 2000;96(6):2140-2148.

27. Drysdale BE, Howard DL, Johnson RJ. Identification of a lipopolysaccharide inducible transcription factor in murine macrophages. *Molecular immunology.* Aug 1996;33(11-12):989-998.

28. Farber JM. A collection of mRNA species that are inducible in the RAW 264.7 mouse macrophage cell line by gamma interferon and other agents. *Mol Cell Biol.* Apr 1992;12(4):1535-1545.

29. Gey M, Wanner R, Schilling C, Pedro MT, Sinske D, Knoll B. Atf3 mutant mice show reduced axon regeneration and impaired regeneration-associated gene induction after peripheral nerve injury. *Open biology.* Aug 2016;6(8).

30. John K, Keshava C, Richardson DL, Weston A, Nath J. Immune response signatures of benzo{alpha}pyrene exposure in normal human mammary epithelial cells in the absence or presence of chlorophyllin. *Cancer genomics & proteomics.* Jan-Feb 2009;6(1):1-11.

31. Mayumi-Matsuda K, Kojima S, Nakayama T, Suzuki H, Sakata T. Scanning gene expression during neuronal cell death evoked by nerve growth factor depletion. *Biochimica et biophysica acta.* Dec 23 1999;1489(2-3):293-302.

32. Nawa T, Nawa MT, Cai Y, et al. Repression of TNF-alpha-induced E-selectin

expression by PPAR activators: involvement of transcriptional repressor LRF-1/ATF3. *Biochemical and biophysical research communications.* Aug 28 2000;275(2):406-411.

33. Okamoto A, Iwamoto Y, Maru Y. Oxidative stress-responsive transcription factor ATF3 potentially mediates diabetic angiopathy. *Mol Cell Biol.* Feb 2006;26(3):1087-1097.

34. Shtil AA, Mandlekar S, Yu R, et al. Differential regulation of mitogen-activated protein kinases by microtubule-binding agents in human breast cancer cells. *Oncogene.* Jan 14 1999;18(2):377-384.

35. Tarn C, Bilodeau ML, Hullinger RL, Andrisani OM. Differential immediate early gene expression in conditional hepatitis B virus pX-transforming versus nontransforming hepatocyte cell lines. *The Journal of biological chemistry.* Jan 22 1999;274(4):2327-2336.

36. Yu R, Shtil AA, Tan TH, Roninson IB, Kong AN. Adriamycin activates c-jun N-terminal kinase in human leukemia cells: a relevance to apoptosis. *Cancer letters.* Oct 1 1996;107(1):73-81.

37. Zimmermann J, Erdmann D, Lalande I, Grossenbacher R, Noorani M, Furst P. Proteasome inhibitor induced gene expression profiles reveal overexpression of transcriptional regulators ATF3, GADD153 and MAD1. *Oncogene.* Jun 8 2000;19(25):2913-2920.

38. Hamdi M, Popeijus HE, Carlotti F, et al. ATF3 and Fra1 have opposite functions in JNK- and ERK-dependent DNA damage responses. *DNA repair.* Mar 1 2008;7(3):487-496.

39. Hartman MG, Lu D, Kim ML, et al. Role for activating transcription factor 3 in stress-induced beta-cell apoptosis. *Mol Cell Biol.* Jul 2004;24(13):5721-5732.

40. Jeong BC, Kim JH, Kim K, Kim I, Seong S, Kim N. ATF3 modulates calcium signaling in osteoclast differentiation and activity by associating with c-Fos and NFATc1 proteins. *Bone.* Feb 2017;95:33-40.

41. Kang Y, Chen CR, Massague J. A self-enabling TGFbeta response coupled to stress signaling: Smad engages stress response factor ATF3 for Id1 repression in epithelial cells. *Molecular cell.* Apr 2003;11(4):915-926.

42. Suganami T, Yuan X, Shimoda Y, et al. Activating transcription factor 3 constitutes a negative feedback mechanism that attenuates saturated Fatty acid/toll-like receptor 4 signaling and macrophage activation in obese adipose tissue. *Circulation research.* Jul 2 2009;105(1):25-32.

43. Xie J, Bliss SP, Nett TM, Ebersole BJ, Sealfon SC, Roberson MS. Transcript profiling of immediate early genes reveals a unique role for activating transcription factor 3 in mediating activation of the glycoprotein hormone alpha-subunit promoter by gonadotropin-releasing hormone. *Molecular endocrinology (Baltimore, Md.).* Oct 2005;19(10):2624-2638.

44. Chen X, Yuan J, Xue G, et al. Translational control by DHX36 binding to 5′UTR G-quadruplex is essential for muscle stem-cell regenerative functions. *Nature Communications.* 2021/08/19 2021;12(1):5043.

45. Sambasivan R, Gayraud-Morel B, Dumas G, et al. Distinct regulatory cascades govern extraocular and pharyngeal arch muscle progenitor cell fates. *Dev Cell.* Jun

2009;16(6):810-821.
46. Taglietti V, Angelini G, Mura G, et al. RhoA and ERK signalling regulate the expression of the transcription factor Nfix in myogenic cells. *Development.* Oct 29 2018;145(21).
47. Wang G, Zhu H, Situ C, et al. p110α of PI3K is necessary and sufficient for quiescence exit in adult muscle satellite cells. *The EMBO journal.* 2018;37(8):e98239.
48. Almada AE, Horwitz N, Price FD, et al. FOS licenses early events in stem cell activation driving skeletal muscle regeneration. *Cell Rep.* Jan 26 2021;34(4):108656.
49. Pasut A, Jones AE, Rudnicki MA. Isolation and culture of individual myofibers and their satellite cells from adult skeletal muscle. *J Vis Exp.* Mar 22 2013(73):e50074.
50. Hüttner SS, Ahrens HE, Schmidt M, et al. Isolation and Culture of Individual Myofibers and Their Adjacent Muscle Stem Cells from Aged and Adult Skeletal Muscle. *Methods Mol Biol.* 2019;2045:25-36.
51. Wolford CC, McConoughey SJ, Jalgaonkar SP, et al. Transcription factor ATF3 links host adaptive response to breast cancer metastasis. *The Journal of clinical investigation.* 2013;123(7):2893-2906.
52. Chen F, Zhou J, Li Y, et al. YY 1 regulates skeletal muscle regeneration through controlling metabolic reprogramming of satellite cells. *The EMBO journal.* 2019;38(10):e99727.
53. Li Y, Yuan J, Chen F, et al. Long noncoding RNA SAM promotes myoblast proliferation through stabilizing Sugt1 and facilitating kinetochore assembly. *Nature communications.* 2020;11(1):2725-2725.
54. Goel AJ, Rieder M-K, Arnold H-H, Radice GL, Krauss RS. Niche Cadherins Control the Quiescence-to-Activation Transition in Muscle Stem Cells. *Cell Reports.* 2017/11/21/ 2017;21(8):2236-2250.
55. Keller C, Hansen MS, Coffin CM, Capecchi MR. Pax3: Fkhr interferes with embryonic Pax3 and Pax7 function: implications for alveolar rhabdomyosarcoma cell of origin. *Genes & development.* 2004;18(21):2608-2613.
56. White RB, Biérinx A-S, Gnocchi VF, Zammit PS. Dynamics of muscle fibre growth during postnatal mouse development. *BMC developmental biology.* 2010;10(1):1-11.
57. Kurosaka M, Naito H, Ogura Y, Machida S, Katamoto S. Satellite cell pool enhancement in rat plantaris muscle by endurance training depends on intensity rather than duration. *Acta Physiol (Oxf).* May 2012;205(1):159-166.
58. Egner IM, Bruusgaard JC, Gundersen K. Satellite cell depletion prevents fiber hypertrophy in skeletal muscle. *Development.* Aug 15 2016;143(16):2898-2906.
59. Abreu P, Mendes SV, Ceccatto VM, Hirabara SM. Satellite cell activation induced by aerobic muscle adaptation in response to endurance exercise in humans and rodents. *Life Sci.* Feb 1 2017;170:33-40.
60. Dungan CM, Murach KA, Frick KK, et al. Elevated myonuclear density during skeletal muscle hypertrophy in response to training is reversed during detraining. *Am J Physiol Cell Physiol.* May 1 2019;316(5):C649-c654.
61. Brett JO, Arjona M, Ikeda M, et al. Exercise rejuvenates quiescent skeletal muscle stem cells in old mice through restoration of Cyclin D1. *Nature Metabolism.* 2020/04/01 2020;2(4):307-317.

62. Vernillo G, Giandolini M, Edwards WB, et al. Biomechanics and physiology of uphill and downhill running. *Sports Medicine.* 2017;47(4):615-629.
63. Dehghani M, Kargarfard M, Rabiee F, Nasr-Esfahani MH, Ghaedi K. A comparative study on the effects of acute and chronic downhill running vs uphill running exercise on the RNA levels of the skeletal muscles PGC1-α, FNDC5 and the adipose UCP1 in BALB/c mice. *Gene.* 2018;679:369-376.
64. Prado F, Aguilera A. Partial depletion of histone H4 increases homologous recombination-mediated genetic instability. *Molecular and cellular biology.* 2005;25(4):1526-1536.
65. Celona B, Weiner A, Di Felice F, et al. Substantial histone reduction modulates genomewide nucleosomal occupancy and global transcriptional output. *PLoS Biol.* Jun 2011;9(6):e1001086.
66. Ghule PN, Xie R-L, Medina R, et al. Fidelity of histone gene regulation is obligatory for genome replication and stability. *Molecular and cellular biology.* 2014;34(14):2650-2659.
67. Skene PJ, Henikoff S. An efficient targeted nuclease strategy for high-resolution mapping of DNA binding sites. *eLife.* 2017/01/12 2017;6:e21856.
68. Kang TZE, Zhu L, Yang D, et al. The elevated transcription of ADAM19 by the oncohistone H2BE76K contributes to oncogenic properties in breast cancer. *The Journal of biological chemistry.* Jan-Jun 2021;296:100374.
69. He L, Ding Y, Zhao Y, et al. CRISPR/Cas9/AAV9-mediated in vivo editing identifies MYC regulation of 3D genome in skeletal muscle stem cell. *Stem Cell Reports.* Oct 12 2021;16(10):2442-2458.
70. Baghdadi MB, Castel D, Machado L, et al. Reciprocal signalling by Notch-Collagen V-CALCR retains muscle stem cells in their niche. *Nature.* May 2018;557(7707):714-718.
71. Baghdadi MB, Firmino J, Soni K, et al. Notch-Induced miR-708 Antagonizes Satellite Cell Migration and Maintains Quiescence. *Cell Stem Cell.* Dec 6 2018;23(6):859-868.e855.
72. Fujimaki S, Seko D, Kitajima Y, et al. Notch1 and Notch2 Coordinately Regulate Stem Cell Function in the Quiescent and Activated States of Muscle Satellite Cells. *Stem Cells.* Feb 2018;36(2):278-285.
73. Verma M, Asakura Y, Murakonda BSR, et al. Muscle Satellite Cell Cross-Talk with a Vascular Niche Maintains Quiescence via VEGF and Notch Signaling. *Cell Stem Cell.* Oct 4 2018;23(4):530-543.e539.
74. Kann AP, Hung M, Wang W, et al. An injury-responsive Rac-to-Rho GTPase switch drives activation of muscle stem cells through rapid cytoskeletal remodeling. *Cell Stem Cell.* 2022/06/02/ 2022;29(6):933-947.e936.
75. Liu Y, Chen Y, Deng X, Zhou J. ATF3 prevents stress-induced hematopoietic stem cell exhaustion. *Frontiers in Cell and Developmental Biology.* 2020;8:585771.
76. Hu Z, Chen K, Xia Z, et al. Nucleosome loss leads to global transcriptional up-regulation and genomic instability during yeast aging. *Genes Dev.* Feb 15 2014;28(4):396-408.
77. Mei Q, Huang J, Chen W, et al. Regulation of DNA replication-coupled histone gene

expression. *Oncotarget.* Nov 7 2017;8(55):95005-95022.

78. Lai WKM, Pugh BF. Understanding nucleosome dynamics and their links to gene expression and DNA replication. *Nature Reviews Molecular Cell Biology.* 2017/09/01 2017;18(9):548-562.

79. Hall JK, Banks GB, Chamberlain JS, Olwin BB. Prevention of muscle aging by myofiber-associated satellite cell transplantation. *Science translational medicine.* 2010;2(57):57ra83-57ra83.

80. Thornell L-E. Sarcopenic obesity: satellite cells in the aging muscle. *Current Opinion in Clinical Nutrition & Metabolic Care.* 2011;14(1).

81. Brack AS, Muñoz-Cánoves P. The ins and outs of muscle stem cell aging. *Skelet Muscle.* 2016;6:1.

82. Lepper C, Conway SJ, Fan CM. Adult satellite cells and embryonic muscle progenitors have distinct genetic requirements. *Nature.* Jul 30 2009;460(7255):627-631.

83. Platt RJ, Chen S, Zhou Y, et al. CRISPR-Cas9 knockin mice for genome editing and cancer modeling. *Cell.* 2014;159(2):440-455.

84. Liu L, Cheung TH, Charville GW, Rando TA. Isolation of skeletal muscle stem cells by fluorescence-activated cell sorting. *Nature protocols.* 2015;10(10):1612-1624.

85. Zhu H, Xiao F, Wang G, et al. STAT3 regulates self-renewal of adult muscle satellite cells during injury-induced muscle regeneration. *Cell reports.* 2016;16(8):2102-2115.

86. Chen X, He L, Zhao Y, et al. Malat1 regulates myogenic differentiation and muscle regeneration through modulating MyoD transcriptional activity. *Cell discovery.* 2017;3(1):1-23.

87. Haeussler M, Schönig K, Eckert H, et al. Evaluation of off-target and on-target scoring algorithms and integration into the guide RNA selection tool CRISPOR. *Genome Biol.* Jul 5 2016;17(1):148.

88. Wang H, Hertlein E, Bakkar N, et al. NF-κB regulation of YY1 inhibits skeletal myogenesis through transcriptional silencing of myofibrillar genes. *Molecular and cellular biology.* 2007;27(12):4374-4387.

89. Diao Y, Guo X, Li Y, et al. Pax3/7BP is a Pax7-and Pax3-binding protein that regulates the proliferation of muscle precursor cells by an epigenetic mechanism. *Cell stem cell.* 2012;11(2):231-241.

90. Kim D, Pertea G, Trapnell C, Pimentel H, Kelley R, Salzberg SL. TopHat2: accurate alignment of transcriptomes in the presence of insertions, deletions and gene fusions. *Genome biology.* 2013;14(4):1-13.

91. Trapnell C, Roberts A, Goff L, et al. Differential gene and transcript expression analysis of RNA-seq experiments with TopHat and Cufflinks. *Nature protocols.* 2012;7(3):562-578.

92. Yu G, Wang LG, Han Y, He QY. clusterProfiler: an R package for comparing biological themes among gene clusters. *Omics.* May 2012;16(5):284-287.

93. Huang DW, Sherman BT, Tan Q, et al. The DAVID Gene Functional Classification Tool: a novel biological module-centric algorithm to functionally analyze large gene lists. *Genome Biol.* 2007;8(9):R183.

94. Lu L, Sun K, Chen X, et al. Genome-wide survey by ChIP-seq reveals YY1 regulation

of lincRNAs in skeletal myogenesis. *The EMBO journal.* 2013;32(19):2575-2588.

95. Langmead B, Salzberg SL. Fast gapped-read alignment with Bowtie 2. *Nature methods.* 2012;9(4):357-359.

96. Zhang Y, Liu T, Meyer CA, et al. Model-based analysis of ChIP-Seq (MACS). *Genome biology.* 2008;9(9):1-9.

97. Ramírez F, Dündar F, Diehl S, Grüning BA, Manke T. deepTools: a flexible platform for exploring deep-sequencing data. *Nucleic acids research.* 2014;42(W1):W187-W191.

Figure Legend

Fig. 1 ATF3 is rapidly and transiently induced during early SC activation. a Schematic for isolation of quiescent satellite cells (QSC) after in situ fixation, freshly isolated SCs (FISC) without prior fixation from muscles of Tg: *Pax7-nGFP* mice. FISCs were subsequently cultured and activated for 24 (ASC-24h), 48 (ASC-48h), or 72 h (DSC-72h). RNAs were extracted for RNA-Seq analysis. **b** Heat maps indicating gene expression levels (Log2[FPKM]) of AP-1 family TFs detected by the RNA-Seq. **c-d** Expression levels (FPKM) and genomic snapshots of *Atf3*, *Atf4*, *Fos*, *FosB*, *JunB* mRNAs from the above RNA-Seq. **e** RT-qPCR detection of *Atf3* in the above cells. **f** Immunofluorescence (IF) staining of ATF3 and Pax7 protein on the above cells. Scale bar: 50 μm. **g** IF staining of ATF3 and Pax7 protein on single myofibers from EDL muscles immediately after isolation or cultured for 24h. Scale bar: 25 μm. All the bar graphs are presented as mean ± SD. *p < 0.05, **p < 0.01, ***p < 0.001. n.s., no significance.

Fig. 2 Short-term *Atf3* deletion accelerates acute injury-induced muscle regeneration. a Breeding scheme for generating inducible *Atf3* inducible conditional knock out (*Atf3* iKO), $Pax7^{CreER/+}$; $ROSA^{EYFP/+}$; $Atf3^{fl/fl}$, and control (Ctrl), $Pax7^{CreER/+}$; $ROSA^{EYFP/+}$; *Atf3*+/+, littermates. **b** Schematic outline of the tamoxifen (TMX) administration used in the study and experimental design for testing the effect of short-term *Atf3* deletion on barium chloride ($BaCl_2$) induced muscle regeneration process. **c** Loss of ATF3 protein in iKO FISC was confirmed by Western blot. α-Tubulin was used as a loading control. **d** No overt morphological difference or body weight change was observed in representative Ctrl vs iKO mice. **e** Left: H&E staining of the TA muscles collected at 3, 5 and 7 days post the 1st round injury (dpi). Scale bar: 50 μm. Right: Cross-sectional areas (CSAs) of newly formed fibers were quantified from the TA muscles at 7dpi and the distribution is shown. n = 3 mice per group. **f** Left: IF staining of eMyHC (red) and Laminin (green) was performed on the above TA muscles. Scale bar: 50 μm. Right: the numbers of eMyHC+ fibers per view at 3dpi were quantified. n = 3 mice per group. **g-h** Left: H&E and eMyHC staining of the TA muscles collected at 3, 5 and 7 days post the 2nd round injury. Scale bar: 50 μm. n = 3 mice per group.

i-j H&E and eMyHC staining of the TA muscles collected at 3, 5 and 7 days post the 3rd round injury. Scale bar: 50 μm. n = 3 mice per group. **k** Left: IF staining of Pax7 (red) and Laminin (green) on Ctrl and iKO TA muscles on 30 days post the 3rd round of injury. Scale bar: 50 μm. Right: the numbers of Pax7+ SCs per view were quantified. n = 3 mice per group. **l** Schematic for engraftment. FISCs from donor mice (Ctrl/ iKO) were injected into pre-injured (1 day before) receptor nude mice. TA muscles were collected 21 days after engraftment for analysis. **m** Left: IF staining of YFP (green) and Laminin (red) on the TA muscles 21 days after engraftment. Scale bar: 50 μm. Right: the numbers of YFP+ fibers per view at 21 days after engraftment were quantified. n= 3 mice per group. **n** IF staining of Myod (red) and Laminin (green) on Ctrl and iKO TA muscles at 3 and 5 days post the 1st, 2nd and 3rd rounds of injury. Scale bar: 50 μm; n = 3 mice per group. **o** Quantification of the numbers of Myod+ SCs per view on the above TA muscles (N). n = 3 mice per group. All the bar graphs are presented as mean ± SD. *p < 0.05, **p < 0.01, ***p < 0.001. n.s., no significance.

Fig. 3 *Atf3* deletion provokes premature SC activation and pseudo-regeneration in homeostatic muscle. a Left: SCs from Ctrl or iKO mice were cultured for 24 h and treated with EdU for 6 h before staining for EdU (red) and Pax7 (green). Scale bar: 50 μm. Right: Quantification of the percentage of EdU+Pax7+ SCs. n = 3 mice per group. **b** Left: IF staining of Pax7 (green) and MyoD (red) on the above SCs cultured for 24 h. Scale bar: 50 μm. Right: Quantification of the percentage of Myod+Pax7+ SCs. n = 3 mice per group. **c** Left: Representative FACS plots showing the size of FISCs sorted from Ctrl or iKO muscles. Right: Quantification of the cell size. n = 3 mice per group. **d** Left: Freshly isolated myofibers from Ctrl or iKO mice were cultured for 36h and treated with EdU for 6h before staining for EdU (red) and Pax7 (green). Scale bar: 50 μm. Right: Quantification of the percentage of EdU+Pax7+ SCs. n = 3 mice per group. **e** IF staining of Pax7 (green) and MyoD (red) on the above myofibers immediately after isolation or cultured for 3h. Scale bar: 25 μm; n = 3 mice per group. **f** Quantification of the percentage of Myod-Pax7+ and Myod+Pax7+ SCs. n = 3 mice per group. **g** Left: IF staining of Pax7 (red) and Laminin (green) on uninjured Ctrl or iKO muscles 5, 21, 28 and 56 days after TMX injection. Scale bar: 50 μm. Right:

Quantification of the numbers of Pax7+ SCs per 100 fibers. n = 3 mice per group. **h** Left: H&E staining of the above uninjured muscles 56 days after TMX injection. Scale bar: 50 μm. Right: Quantification of the numbers of CLN fibers per section. n = 3 mice per group. **i** Upper: Schematic outline of the in vivo EdU assay performed on uninjured Ctrl or iKO muscle; EdU was injected by IP 5 days after TMX. The muscles were collected 21 days later. Lower Left: IF staining of EdU (red) and Laminin (green). Scale bar: 25 μm. Lower Right: Quantification of the number of EdU+ cells per section. n = 3 mice per group. **j** Upper: Schematic outline of the EdU assay performed in the study; EdU was injected by IP 5 days after TMX, TA muscle and myofibers were collected 12h later. Lower Left: EdU (red) and Pax7 (green) staining on freshly single myofibers from the above injected muscles; Lower Right: EdU (red) and YFP (green) staining on the above muscles 12h after EdU injection. Scale bar: 25 μm; n = 3 mice per group. **k** Left: IF staining of Myod (green) and MyoG (red) on single myofibers isolated from Ctrl or iKO mice and cultured for 72h. Scale bar: 50 μm. Right: Quantification of the percentage of the Myod+MyoG+ SCs. n = 3 mice per group. **l** Left: IF staining of Pax7 (green) and Myod (red) on the above single myofibers. Scale bar: 50 μm. Right: Quantification of the percentage of Pax7+Myod+ SCs. n = 3 mice per group. All the bar graphs are presented as mean ± SD. *p < 0.05, **p < 0.01, ***p < 0.001. n.s., no significance.

Fig. 4 Long-term *Atf3* deficiency depletes SC pool and impairs muscle regeneration. A Schematic outline of the experimental design for testing the effect of long-term *Atf3* deletion on muscle regeneration process. **a** 30 or 120 days chasing after TMX injection was given before $BaCl_2$ injection. **b** Left: H&E staining of the TA muscles collected at 3, 5 and 7 dpi after the 30 days chasing period. Scale bar: 50 μm. n = 3 mice per group. Right: CSAs of newly formed fibers were quantified from the above-stained TA muscle at 7dpi and the distribution is shown. n = 3 mice per group. **c** Left: IF staining of eMyHC (red) and Laminin (green) was performed on the above TA muscles. Scale bar: 50 μm. Right: Quantification of the numbers of eMyHC+ fibers per view at 5 and 7dpi. n = 3 mice per group. **d** Left: IF staining of Pax7 (red) and Laminin (green) was performed on the above TA muscles. Scale

bar: 50 μm. Right: Quantification of the numbers of Pax7+ SCs per view. n = 3 mice per group. **e-g** The above assays/quantifications were performed on the Ctrl or iKO muscles collected at 3, 5 and 7 dpi after the 120 days chasing period. Scale bar: 50 μm. n = 3 mice per group. All the bar graphs are presented as mean ± SD. *p < 0.05, **p < 0.01, ***p < 0.001. n.s., no significance.

Fig. 5 *Atf3* deletion induces SC activation during voluntary and resistance exercise. a Schematic outline of the experimental design for testing SC activities in voluntary exercise (VE). After TMX injection, Ctrl or iKO mice were trained on voluntary running wheels for 1 week and followed by 3 more weeks of running and recording. TA muscles and FISCs were then collected for staining and EdU assays respectively. **b** Left: IF staining of Myod (red) and Laminin (green) was performed on the TA muscles collected from Ctrl or iKO mice with or without VE. Scale bar: 50 μm. Right: Quantification of the numbers of Myod+ cells per section. n = 3 mice per group. **c** Left: IF staining of Pax7 (green) and MyoD (red) on SCs isolated from the above mice and cultured for 24 h sorted. Scale bar: 50 μm. Right: Quantification of the percentages of Myod+/Pax7+ SCs; n = 3 mice per group. **d** Left: SCs were sorted from the above mice with or without VE and cultured for 24 h. EdU was then added to the culture medium 6h before staining for EdU (red). Scale bar: 50 μm. Right: Quantification of the percentage of EdU+ SCs; n = 3 mice per group. **e** Left: H&E staining of the TA muscles collected from the above Ctrl and iKO mice with or without VE. Scale bar: 50 μm. Right: Quantification of the numbers of CLN fibers per section; n = 3 mice per group. **f** Quantifications of the fiber size of the above-stained TA muscles (e); n = 3 mice per group. **g** Left: IF staining of Pax7 (red) and Laminin (green) on the above collected TA muscles Scale bar: 50 μm. Right: Quantification of the numbers of Pax7+ SCs per 100 fibers; n = 3 mice per group. **h** Schematic outline of the experimental design for testing the SC activities after resistance exercise (RE). After TMX injection, Ctrl or iKO mice were trained on a treadmill with a 5° incline at a speed of 20 cm/sec for 60min for 5 days and followed by 10 more days of running and recording. TA muscles and FISCs were then collected for staining and EdU assays respectively. **i** Left: IF staining of Myod (red) and Laminin (green) on the TA muscles

collected from the above Ctrl and iKO mice with or without RE. Scale bar: 50 μm. Right: Quantification of the numbers of Myod+ cells per section; n = 3 mice per group. **j** Left: IF staining of Pax7 (green) and MyoD (red) on SCs sorted from the above mice and cultured for 24 h. Scale bar: 50 μm. Right: Quantification of the percentage of Myod+/Pax7+ SCs; n = 3 mice per group. **k** Left: SCs were isolated from the above mice and cultured for 24 h. EdU was then added to the culture medium 6h before staining for EdU (red). Scale bar: 50 μm. Right: Quantification of the percentage of EdU+ SCs; n = 3 mice per group. **l** Left: H&E staining of the above collected TA muscles with or without RE. Scale bar: 50 μm. Right: Quantification of the numbers of CLN fibers per section; n = 3 mice per group. **m** Quantification of the fiber size of the above-stained TA muscles (l); n = 3 mice per group. **n** Left: IF staining of Pax7 (red) and Laminin (green) on the above collected TA muscles. Scale bar: 50 μm. Right: Quantification of the numbers of Pax7+ SCs per 100 fibers; n = 3 mice per group. All the bar graphs are presented as mean ± SD. *p < 0.05, **p < 0.01, ***p < 0.001. n.s., no significance.

Fig. 6 ATF3 regulates *H2B* gene expression and nucleosome patterning. a Schematic outline of the experimental design. RNA-Seq and H2B CUT&RUN were performed with FISCs isolated from Ctrl or iKO mice; ATF3 ChIP-Seq was performed with C2C12 overexpressing ATF3. The acquired datasets were then integrated for analyses. **b** Left: Differentially expressed genes (DEGs) were identified from the above Ctrl vs. iKO RNA-Seq. Right: The percentages of up and down-regulated genes. **c&d** Gene ontology (GO) analyses of the above up and down-regulated genes. The top 5 enriched GO terms ranked by gene ratio (proportion of genes annotated for each GO term) are shown. Dots are colored by adjusted P value of fold change (FC) and their size corresponds to the gene counts annotated to each GO term. **e** FPKM and Log2FC of *H2b* genes in iKO vs. Ctrl from the above RNA-Seq. **f** ChIP-Seq was performed using chromatins from C2C12 cells overexpressing ATF3, and the genomic distribution of 2871 ATF3 binding peaks is shown. **g** *De novo* motif prediction by DREME revealed the enrichment of canonical ATF3 motifs in the above binding regions. **h** The GO analysis for all the above genes with ATF3 binding. The top ten enriched GO terms

ranked by gene ratio are shown. Dots are colored by adjusted P value (degree of enrichment) and their size corresponds to the gene counts annotated to each GO term. **i** Left: Venn diagrams showing the overlapping (72 genes) between the above identified ChIP-Seq target (2871) and the down-regulated genes (469) from the RNA-Seq. Right: GO analysis of the above 72 genes revealed an extreme enrichment of histone-related terms. **j** Genomic snapshots of 3 of the above identified *H2b* genes (*Hist1h2bb*, *Hist1h2bm* and *Hist2h2bb*) with ATF3 binding in their TSSs (ChIP-Seq tracks) and down-regulated by ATF3 deletion (RNA-Seq tracks). **k** ATF3, H2A, H2B, H3 and H4 proteins were measured by western blot in FISC from Ctrl and iKO mice. α-Tubulin was used as a loading control. **l** IF staining of H2A (green) and H2B (red) on the above FISCs. Scale bar: 100 μm; n = 3 mice per group. **m** H2B CUT&RUN was performed with FISCs isolated from Ctrl or iKO mice. The enrichment level in iKO vs. Ctrl was compared by analyzing gains and losses of H2B reads (fold change 1.5) in 10 kb bins. Pie charts showing the number of the bins with H2B changed (6589, 229 up and 6369 down) and unchanged (247114) (left and middle), and the genomic distribution of the down-regulated H2B signals (right). **n** Genomic snapshots of a 1098kb region Integrative Genomics Viewer (IGV) track of H2B signal in-Ctrl vs. iKO in Chr4. **o** Schematic of the RNA Polymerase II elongation process during DNA transcription **p** Venn diagrams showing the overlapping (252 genes) between the above regions with down-regulated H2B CUT&RUN signals (4333) and the up-regulated genes (1866) from the above (A) RNA-Seq. **q** Metaplots showing average H2B CUT&RUN signals in Ctrl and iKO cell 3 kb upstream to 3 kb downstream of TSS. **r** GO analysis of the above 252 genes from (P). The top ten enriched GO terms ranked by gene ratio are shown. Dots are colored by adjusted P value (degree of enrichment) and their size corresponds to the gene counts annotated to each GO term. **s** Genomic snapshots of *Eln* gene which shows down-regulated H2B CUT&RUN signal and up-regulated RNA-Seq signal in iKO vs. Ctrl. Regions with H2B signal reduction in iKO vs. Ctrl are highlighted in blue frame.

Fig. 7 H2B loss increases DNA damage and senescence in *Atf3* iKO SCs. a Upper: Comet assay was performed on Ctrl or iKO SCs after 0, 1000 or 2000J UV treatment. Scale bar: 25

μm. Lower: Quantification of the length of comet tails; n = 3 mice per group. **b** IF staining of γH2AX (red) and Myod (green) was performed on SCs from Ctrl or iKO mice after cultured for 0, 24, 48 or 72hours. Scale bar: 50 μm. **c** Quantification of the percentages of Myod+ / γH2AX+ cells; n = 3 mice per group. **d** Left: β-Gal (blue) staining was performed on SCs from Ctrl or iKO mice after cultured for 9 days. Scale bar: 50 μm. Right: Quantification of the percentages of β-Gal+ cells; n = 3 mice per group. **e** Expression of the selected senescence marker genes including *p16*, *p21* and *p53* in SCs from Ctrl and iKO was quantified by RT–qPCR**. f** p21 and p53 protein levels were detected by Western blotting in SCs from Ctrl and iKO mice. GAPDH was used as a loading control. **g&h** SCs from Ctrl and iKO mice were transfected with an H2B-overexpression or vector control plasmid. 96hours after transfection, expression of the indicated genes was detected by Western blotting and RT–qPCR. GAPDH was used as a loading control. **i** Left: The above transfected cells were cultured for 24 h before treated with EdU for 6 h and stained for EdU (red) and Pax7 (green). Scale bar: 50 μm. Right: Quantification of the percentage of EdU+/Pax7+ SCs; n = 3 mice per group. **j** Schematic model depicting the functional role of ATF3 in preserving SC quiescence and preventing SC precocious activation. In homeostatic muscle, the rapid induction of ATF3 upon minor stress promotes *H2b* expression to maintain proper nucleosome positioning and suppress the expression of activation genes, thus preventing the precocious activation of SCs. With ATF3 loss, H2B deficiency occurs which leads to altered nucleosomes positioning and the up-regulation of activation genes, causing SCs to break quiescence (QSC) and enter early activating stage (eASC). All the bar graphs are presented as mean ± SD. *p < 0.05, **p < 0.01, ***p < 0.001. n.s., no significance.

Figure 1. Zhang S et. al.

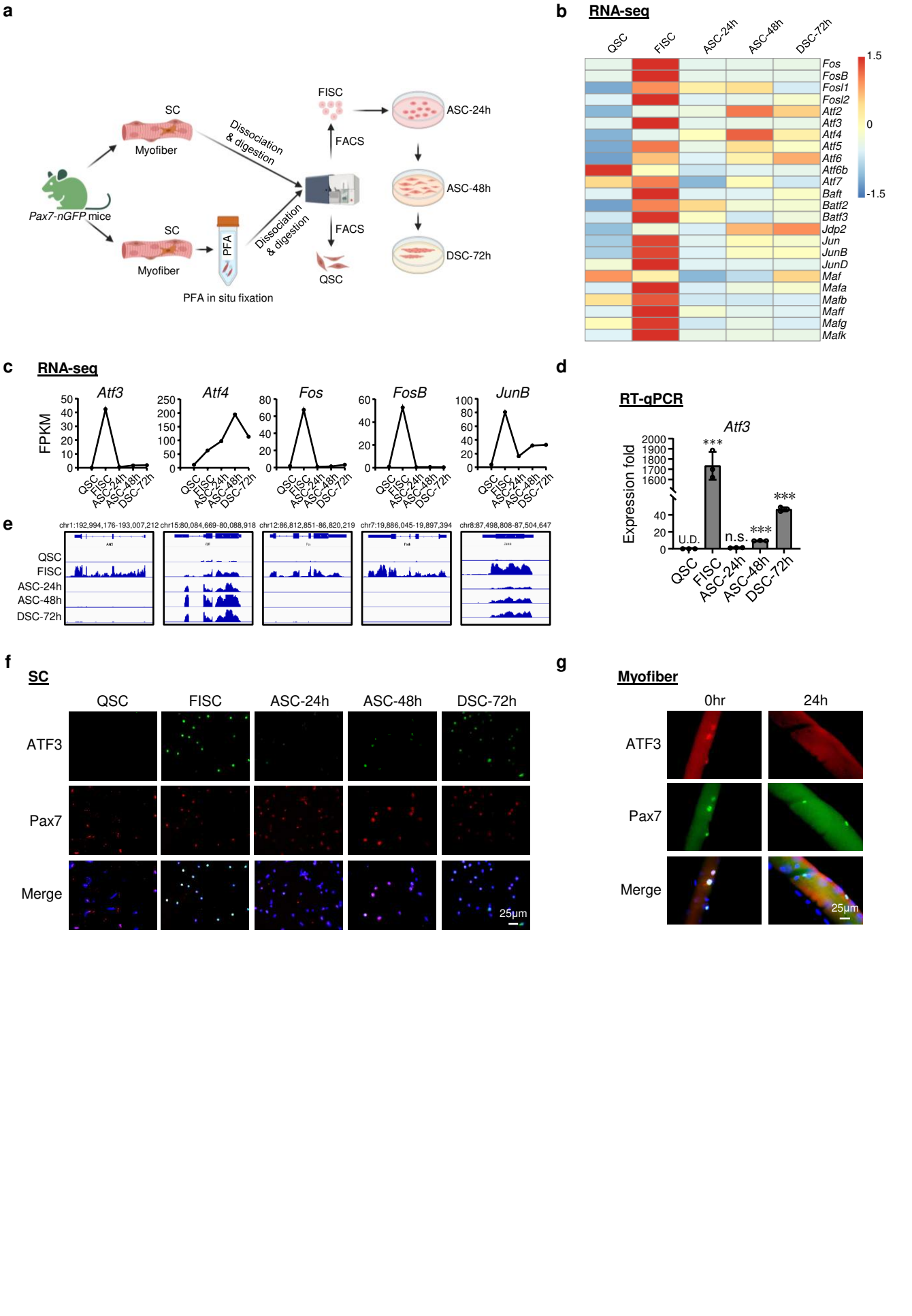

Figure 2. Zhang S et. al.

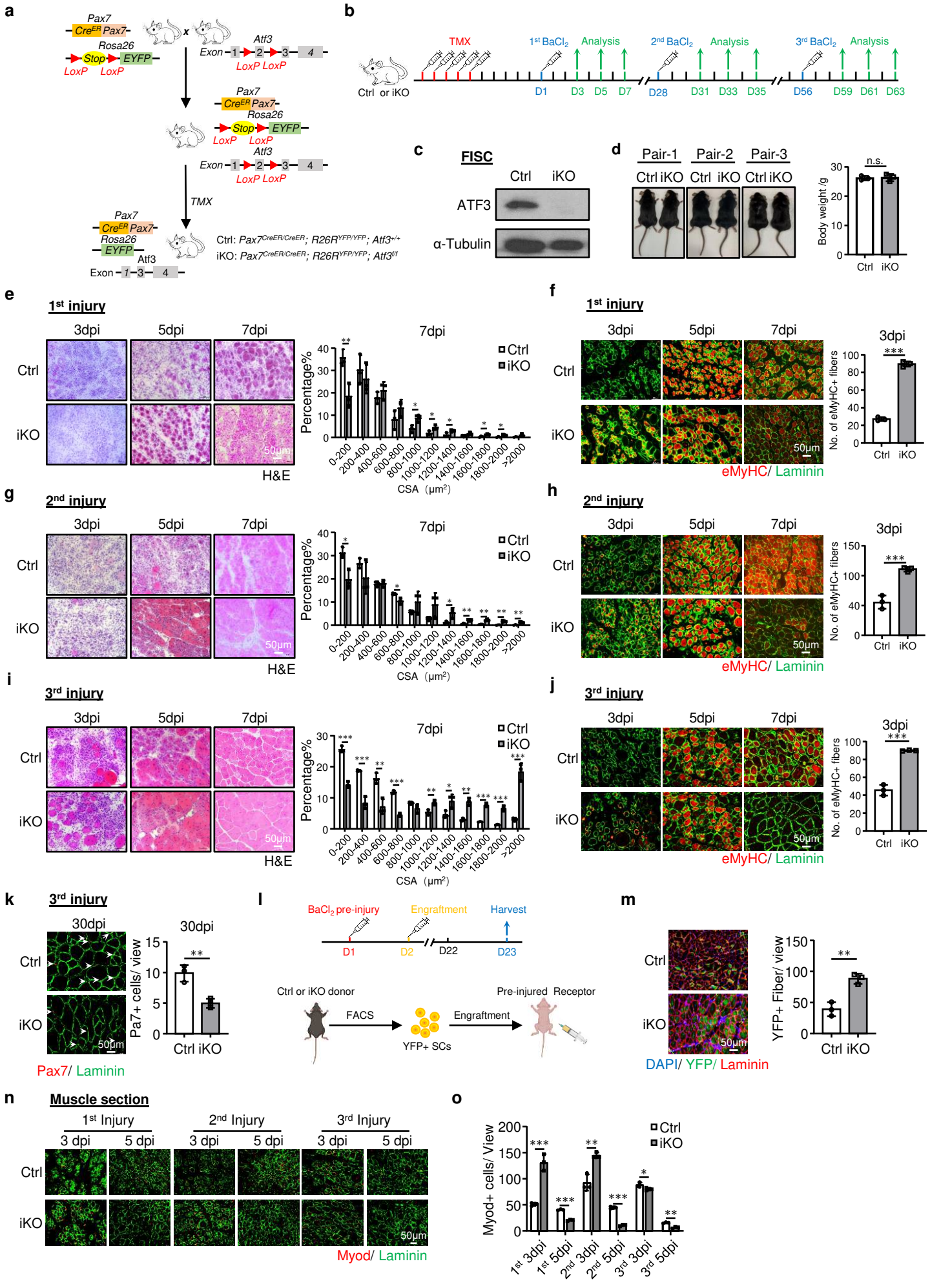

Figure 3. Zhang S et. al.

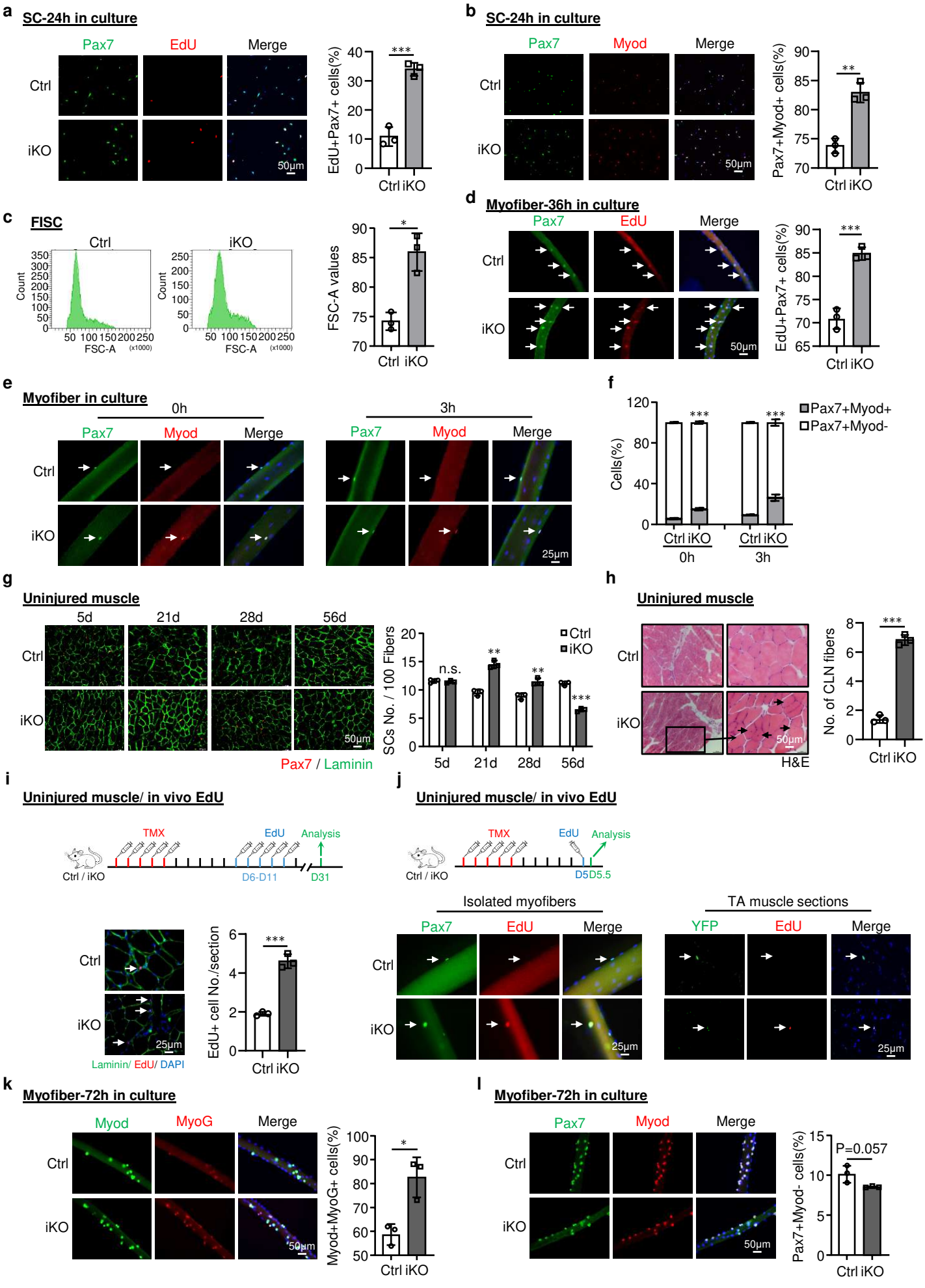

Figure 4. Zhang S et. al.

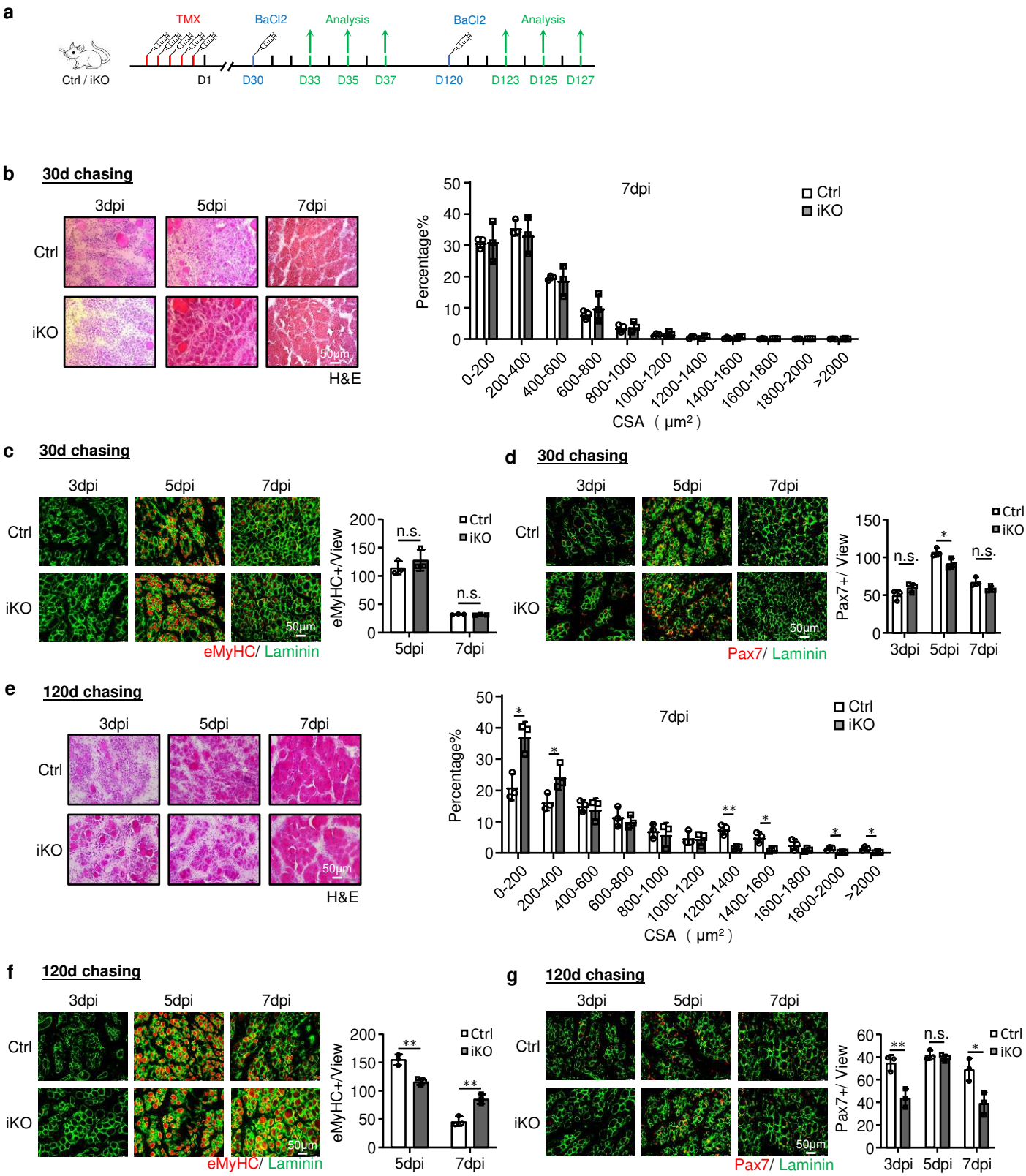

Figure 5. Zhang S et. al.

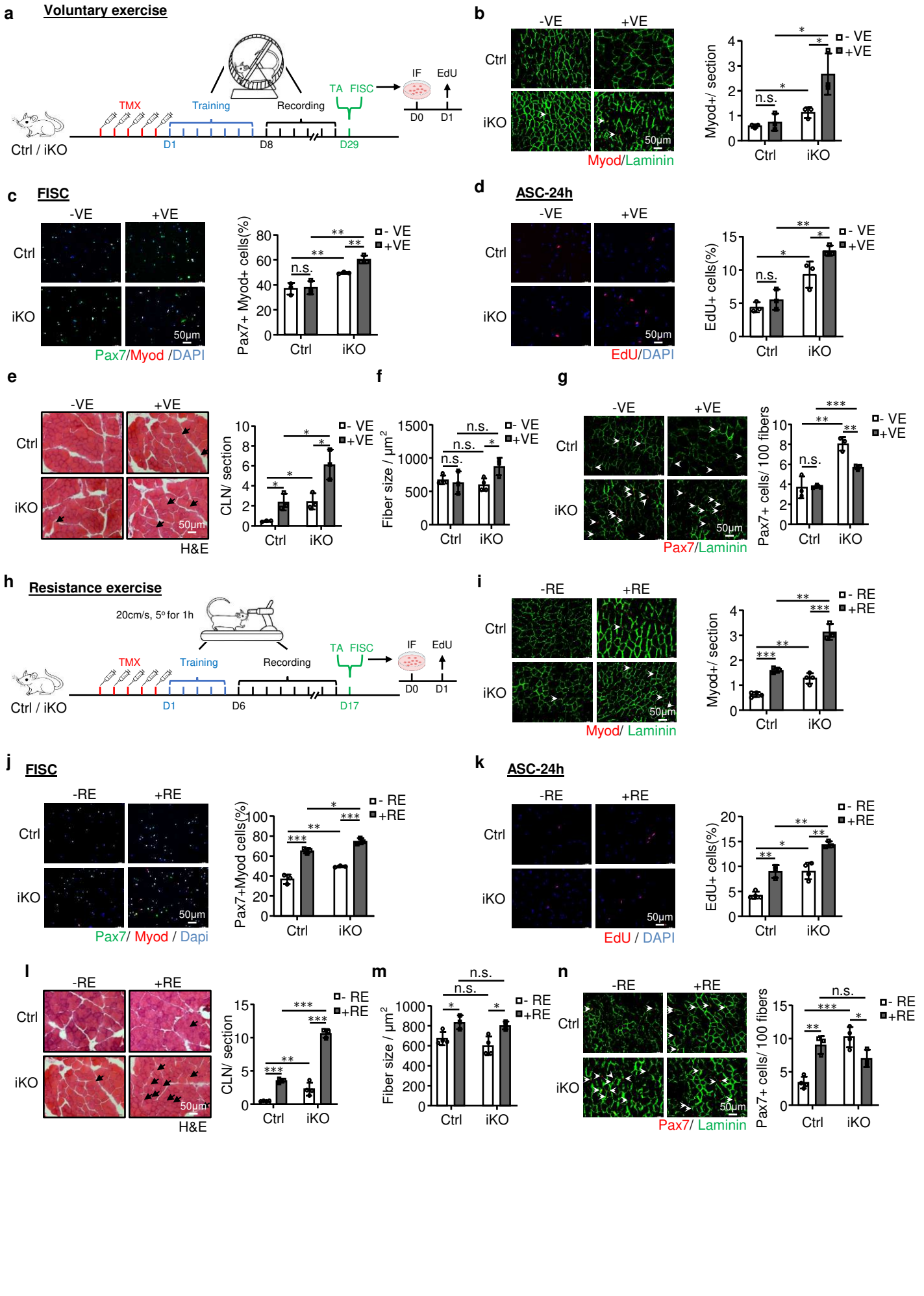

Figure 6. Zhang S et. al.

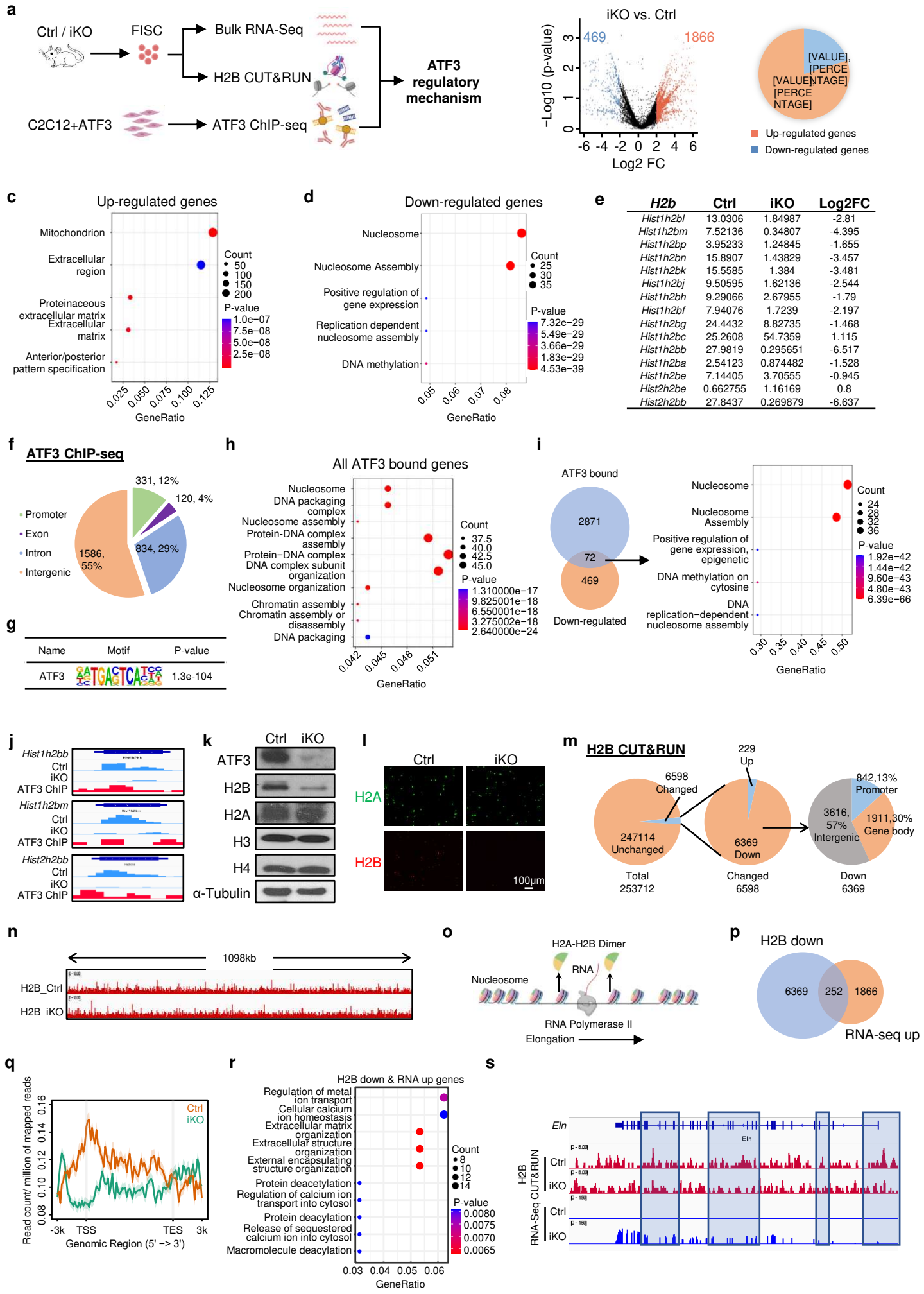

H2b	Ctrl	iKO	Log2FC
Hist1h2bl	13.0306	1.84987	-2.81
Hist1h2bm	7.52136	0.34807	-4.395
Hist1h2bp	3.95233	1.24845	-1.655
Hist1h2bn	15.8907	1.43829	-3.457
Hist1h2bk	15.5585	1.384	-3.481
Hist1h2bj	9.50595	1.62136	-2.544
Hist1h2bh	9.29066	2.67955	-1.79
Hist1h2bf	7.94076	1.7239	-2.197
Hist1h2bg	24.4432	8.82735	-1.468
Hist1h2bc	25.2608	54.7359	1.115
Hist1h2bb	27.9819	0.295651	-6.517
Hist1h2ba	2.54123	0.874482	-1.528
Hist1h2be	7.14405	3.70555	-0.945
Hist2h2be	0.662755	1.16169	0.8
Hist2h2bb	27.8437	0.269879	-6.637

Figure 7. Zhang S et. al.

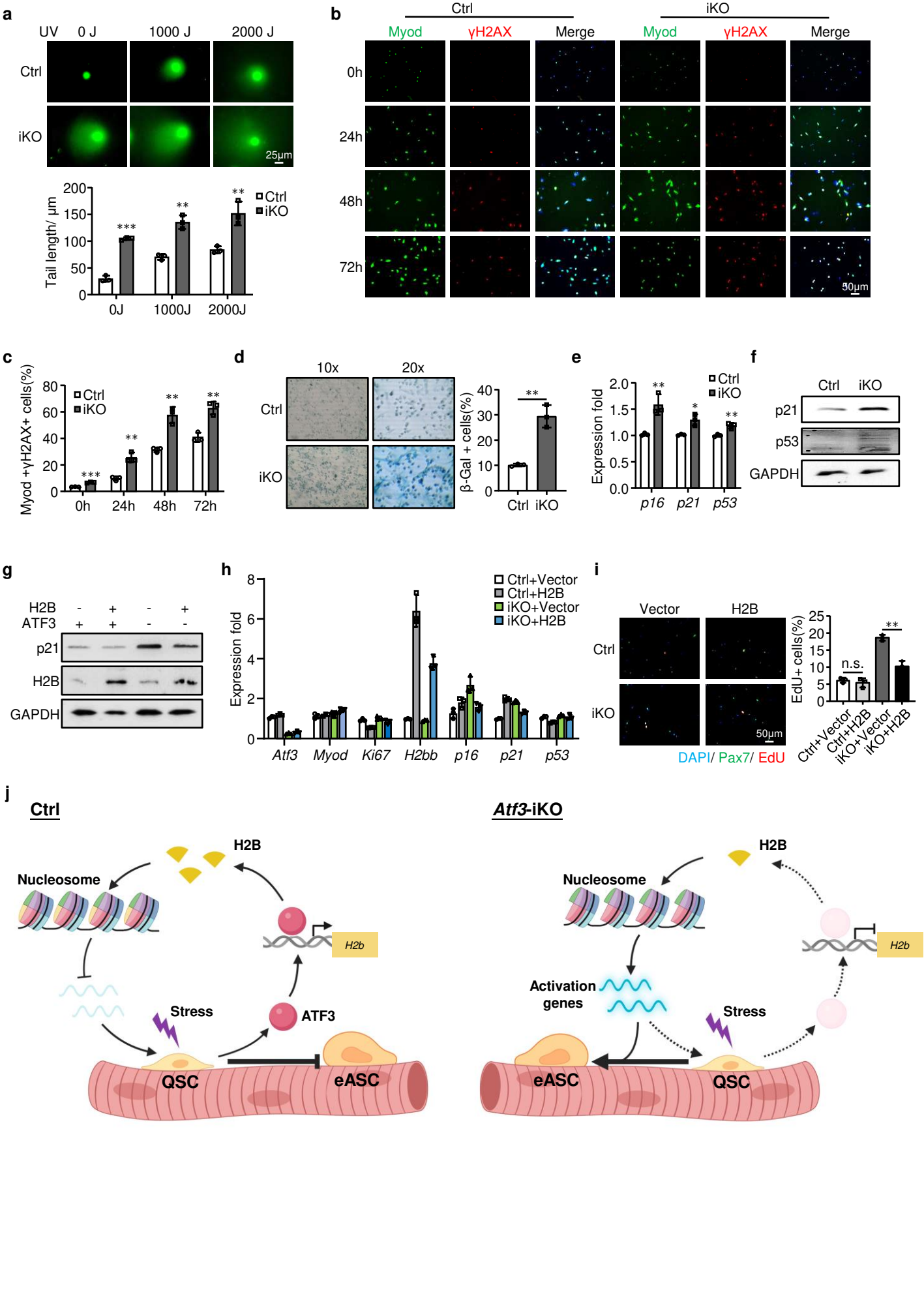

Supplementary Files

This is a list of supplementary files associated with this preprint. Click to download.

- Atf3SupplInfo.pdf
- TableS1iKORNAseq.xlsx
- TableS2ChIPseq.xlsx
- TableS3cKORNAseq.xlsx
- TableS4H2Bdown.xlsx
- TableS5Oligonucleotidesused.xlsx